國立交通大學

應用化學系分子科學碩士班

碩 士 論 文

飛秒雷射誘發胺基酸與蛋白質於氣液介面結晶化之研究

Femtosecond Laser-Induced Crystallization of Amino Acid

and Protein at the Air/Solution Interface

研 究 生：劉 宗翰 (Tsung-Han Liu)

指導教授：增原 宏 博士 (Dr. Hiroshi Masuhara)

中 華 民 國 一 百 年 七 月

飛秒雷射誘發胺基酸與蛋白質於氣液介面結晶化
Femtosecond Laser-Induced Crystallization of Amino Acid
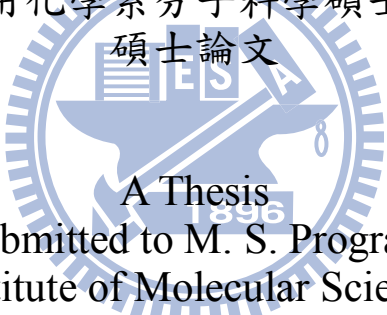and Protein at the Air/Solution Interface

研 究 生：劉宗翰　　　　　Student：Tsung-Han Liu

指導教授：增原宏 博士　　　Advisor：Dr. Hiroshi Masuhara

國立交通大學
應用化學系分子科學碩士班
碩士論文

A Thesis
Submitted to M. S. Program
Institute of Molecular Science
Department of Applied Chemistry
National Chiao Tung University
in partial Fulfillment of the Requirements
for the Degree of
Master
in

Molecular Science

July 2011

Hsinchu, Taiwan, Republic of China

中 華 民 國 一 百 年 七 月

飛秒雷射誘發胺基酸與蛋白質於氣液介面結晶化之研究

研究生：劉宗翰　　　　　　　　　　指導教授：增原宏 博士

國立交通大學

應用化學系分子科學碩士班

摘要

　　使用雷射誘使結晶化的發生已成為現今取得分子結晶相當重要的技術，特別是已於 2002 年被成功示範的飛秒雷射誘使結晶化技術，現正往蛋白質結晶迅速發展。當高強度的雷射脈衝被聚焦於過飽和水溶液之中，水的多光子吸收現象發生，並對周圍環境產生機械性壓力波，最後致使溶質結晶。於本研究中，我們探討飛秒雷射參數如脈衝能量、脈衝頻率與聚焦位置對結晶化與取得結晶的影響，並示範利用聚焦雷射於溶液表面可有效提升分子結晶的機率。

　　在第一部分，我們示範飛秒雷射誘發甘胺酸過飽和溶液結晶化並檢驗雷射參數與結晶機率、結晶形貌和晶相的關係。脈衝能量與頻率的依存性實驗結果顯示結晶形貌與數量主要是由水的多光子吸收現象引發的空穴氣泡產生頻率所決定。此外，藉由聚焦雷射脈衝於空氣溶液介面可大幅增進結

晶機率，其原因被推斷可能為甘胺酸分子於介面的分子吸附，並依此推論以我們所知首次成功示範使用單發雷射脈衝誘發甘胺酸單晶的產生。

於第二部分，我們以類似上述的方式示範飛秒雷射誘發於蛋白質結晶學中最標準的酵素與蛋白質-溶菌酶過飽和溶液結晶化。我們發現相較於聚焦雷射在溶液液滴中與自然結晶的條件下，聚焦雷射在溶液液滴的空氣溶液介面可顯著地增進結晶機率。另從各條件下取得之結晶的 X-ray 繞射分析結果可得知其晶格結構並無差異。儘管有研究指出蛋白質會吸附於溶液表面且會致使蛋白質變性，但實驗結果顯示鹽析效應可穩定蛋白質於溶液介面的結構，而相關的當代研究亦支持此結果。

目前的研究結果表示於飛秒雷射誘發結晶化中使用雷射照射溶液表面可改善現存的結晶技術。分子在溶液表面成核的初期階段的進一步光譜動態研究可望從此結晶方法建立新穎的表面/介面分子科學。

Femtosecond Laser-Induced Crystallization of

Amino Acid and Protein at the Air/Solution Interface

Student: Tsung-Han Liu   **Advisor: Dr. Hiroshi Masuhara**

M. S. Program

Institute of Molecular Science

Department of Applied Chemistry

National Chiao Tung University

Abstract

Laser-induced crystallization is now becoming an indispensable technique to obtain molecular crystal. Particularly, femtosecond (fs) laser-induced crystallization was demonstrated in 2002 and is developing especially toward protein crystallization technique. When an intense fs laser pulse is focused into a supersaturated solution, multiphoton absorption of solvent occurs and induces mechanical stress to the surrounding area, which results in crystallization of solute. In this study, we explore how fs laser parameters such as pulse energy, repetition rate, and focal position affect crystallization and obtained crystals, and then demonstrate that solution surface irradiation of fs laser pulses can improve molecular crystallization probability drastically.

Firstly, fs laser induced crystallization of glycine from the supersaturated solution is demonstrated and relations among laser parameters and crystallization probability, crystal morphology, and the polymorph are examined. Pulse energy and repetition rate dependences

show that the frequency of cavitation bubble generation induced by multiphoton absorption of water mainly determines crystal morphology and number. Furthermore, significant increase of crystallization probability is also demonstrated by focusing fs pulses at the air/solution interface, whose mechanism may be ascribed to molecular adsorption at the interface. Based on the inference, we have succeeded in single glycine crystal formation induced by single fs pulse irradiation for the first time as far as we know.
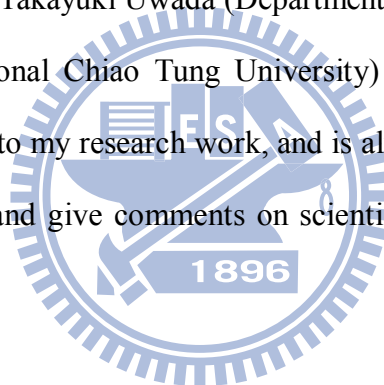
Secondly, we demonstrate fs laser induced crystallization of lysozyme as the most standard enzyme and protein in protein crystallography in the similar manner to glycine. It is revealed that irradiation at the air/solution interface of the solution droplet much improved the crystallization probability, compared with that of fs laser irradiation inside the solution and that of spontaneous crystallization. X-ray diffraction analysis of the obtained crystals clarified that crystal structure was the same under each crystallization condition. It is known that protein can be adsorbed and be localized at the solution surface leading to the denaturation. However, this result indicates that the salting-out effect can stabilize the structure even at the surface, which is contemporarily reported in elsewhere.

The present result clearly shows that utilizing solution surface irradiation in the fs laser-induced crystallization sharpens the existent crystallization technique. Further spectroscopic dynamics study on the early stage of molecular nucleation occurring at the surface is promising to establish novel interface/surface molecular science from this crystallization methodology.

Acknowledgement

Table of Contents

List of Figures

Chapter 3 Experiment

Chapter 4 Glycine Crystallization

Chapter 5 Application to Protein

List of Tables

Chapter 4 Glycine Crystallization

Chapter 5 Application to Protein

Chapter 1

Introduction

Laser light is regarded as a monochromatic light source showing high energy density with high degree of spatial and temporal coherence. Laser beam can be focused to a very tiny spot, and can be delivered at a large distance with extremely low divergence [1]. Therefore, laser exhibits high potential and has been applied widely in diverse fields inclusive of physics, chemistry, material science and so on. Undoubtedly, laser also plays an essential role in various contemporary and interdisciplinary studies.
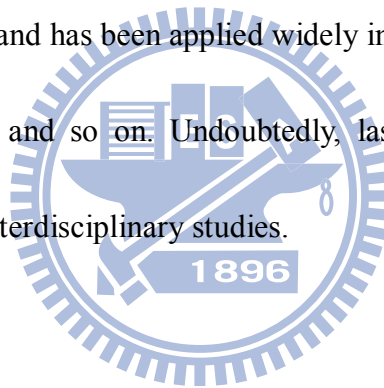
As one of laser applications, photoetching, an essential technique for microfabrications, was first demonstrated when a pulsed ultraviolet excimer laser light with high enough intensity was irradiated at a surface of organic polymer film and some morphological changes were induced [2, 3]. Laser ablation was given to describe this phenomenon induced by pulse laser irradiation at a solid material with intensity higher than a threshold [4]. If laser ablation takes place in liquid or gaseous phase, the phenomenon is usually described as optical breakdown. In fact, optical breakdown can be generated in water when focused femtosecond laser pulses with high intensity are irradiated inside water [5]. The accompanying phase

transition of water from liquid to gas gives transient mechanical stress. The optical breakdown has been employed for biological applications such as cellular surgery [6, 7], and the consequent mechanical stress is applied to cellular arrangement or micropatterning [8] and nanoparticle injection to single cells [9]. Nowadays, the application of optical breakdown has been expanding to the studies on crystallization and crystal growth and has received much attention [10-13].

Crystal is a solid material composed of atoms, molecules or even macromolecules which are three-dimensionally arranged in a long-range order, and crystallization is the process from atoms or molecules to a crystal. Making crystal is not only an important technique for purification and separation, but also an indispensable process in determining crystal structures both of inorganic solid-state materials and biological molecular crystals at atomic resolution with X-ray diffraction analysis [14].

Among the biological macromolecules inclusive of proteins, nucleic acids and carbohydrates, proteins constitute the largest group. Enzymes are the most diverse class of proteins because nearly every chemical reaction in a cell requires a specific enzyme. In order to understand cellular processes or design new structure-based drugs or pharmacological agents, knowledge of the three-dimensional structure, functions and properties of enzymes

and other macromolecules are undoubtedly vital [15, 16]. X-ray diffraction of crystals and

nuclear magnetic resonance (NMR) are two widely-used techniques for the structural

determination of macromolecules at atomic resolution. While NMR does not require protein

crystals and provides more detailed information on the dynamics of the molecule in question,

it can be used only for biopolymers with molecular weight of less than 30,000. X-ray

crystallography can be applied to compound with molecular weight up to at least 10^6. For

many proteins, the difference is decisive in favor of X-ray diffraction [15]. Accordingly, a

major challenge to the full exploitation of X-ray diffraction technique is that the protein must

first be crystallized [16].

Protein crystallization is mainly a trial-and-error procedure in which protein is slowly

precipitated from its solution, so obtaining suitable single crystals is the least understood step

in the X-ray structural analysis of a protein [15]. As a matter of fact, there are still some

additional requirements for the crystallinity and size of the crystals if precise analysis results

are more likely to be obtained [17]. Moreover, since crystallization is a rate-limiting step from

single molecules to a crystal for some proteins such as membrane proteins which can be

attributed to inherent protein flexibility and to conformational inhomogeneity, it is also

necessary to shorten the crystallization time and elevate the crystallization possibility

simultaneously [18]. Therefore, laser-induced crystallization methods as novel crystallization

techniques have received much attention and have been proposed continually to try to satisfy the present situation.

1.1 Introduction to conventional crystallization methods

Because amino acids are polar molecules, most of them can be dissolved well in water rather than organic solvent. Accordingly, water is often used as solvent in crystallization. In an aqueous solution at pH near isoelectric point, amino acids are in zwitterionic form, and their zwitterionic property is still kept in crystal. For crystallization, general methods such as cooling down saturated solution slowly, evaporating saturated solution slowly with adding polar solvent such as alcohol, adding poor solvent into saturated solution, and adjusting pH to lower the solubility of the solution are often used. If crystals with high quality are more likely to be obtained, slow crystal growth at low supersaturated degree is preferred [14].

The history of protein crystal growth can be traced back about more than 150 years ago. The first observed protein crystallization was published by Hünefeld in 1840, and the protein was hemoglobin from earthworm. The crystals were obtained when the blood of an earthworm was pressed between two slides of glass and allowed to dry very slowly. The above description revealed that protein crystals can be obtained by controlling evaporation of a concentrated protein solution. In other words, protein crystals can be produced by slow

dehydration which is one of the most acceptable concepts until now. Other conventional methods such as temperature variation under otherwise constant conditions, the use of salt or organic solvents as precipitating or crystallizating agents, and the use of metal ions were also developed in the following decades [19].

The oldest crystallization technique is batch method which has been used for proteins and nucleic acids crystallization for over 150 years and is regarded as one of the most reliable crystallization methods. Batch method is attractive and convenient because of its inherent simplicity and reproducibility. It requires nothing more than direct mixing of an unsaturated protein solution with a precipitant solution and waiting for a period of time until spontaneous nucleation commences. For instance, lysozyme, the most widely studied protein for protein crystallization, is easily crystallized by batch method [19].

The most commonly used technique for protein crystallization is vapor diffusion inclusive of hanging drop and sitting drop methods. Both of these two methods contain sample solution and reservoir solution, and require a closed environment. At the early stage, the sample solution has insufficient precipitate concentration for crystallization. After vapor diffusion of solvent from sample solution to reservoir solution takes place and vice versa, the precipitate concentration is slowly adjusted to an optimal degree for crystallization since the

amounts of solution are quite different between these two [14].
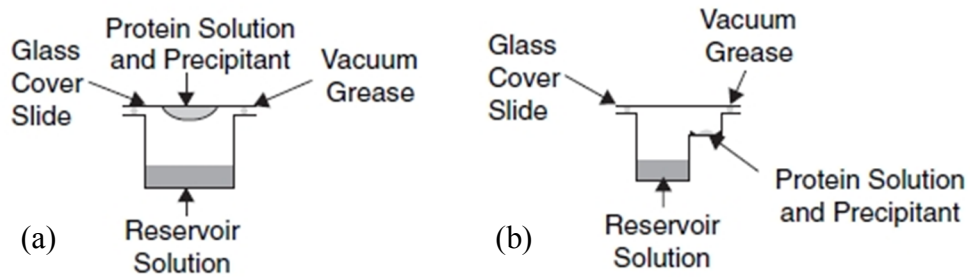
Fig. 1.1 Vapor diffusion for protein crystallization. (a) hanging drop method (b) sitting drop method

1.2 Introduction to crystallization process

Fig. 1.2 shows a schematic illustration of crystal formation from a disordered medium. Compared with the final crystal phase, the initial disordered phase has higher free energy. Crystallization starts from nucleation, in which a tiny embryo of a highly ordered phase with lower free energy is formed. Nucleation seldom takes place spontaneously at unsaturated concentration since it is relatively difficult for molecules to overcome some energy barriers between these two phases. However, at high enough supersaturation, the energy barriers decrease and the initial state becomes unstable, so that a tiny fluctuation can lead to the
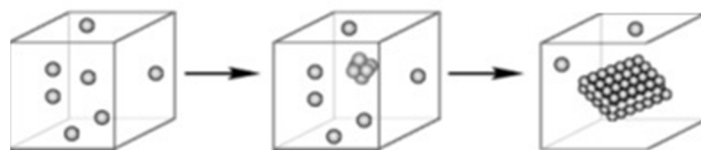
Fig. 1.2 Schematic illustration of crystal formation from a disordered medium to a highly ordered phase [20].

6

appearance of the new phase [20].

An illustration of phase separation during nucleation in detail is shown in Fig. 1.3. There are two possible pathways from individual molecules to nucleation. When the size of molecule accumulation increases to a critical size, the ordered nucleus forms and starts to form crystal. On the other hand, dense liquid droplet or liquid-liquid phase separation formation can be observed if the size of molecule accumulation continuously increases [20].
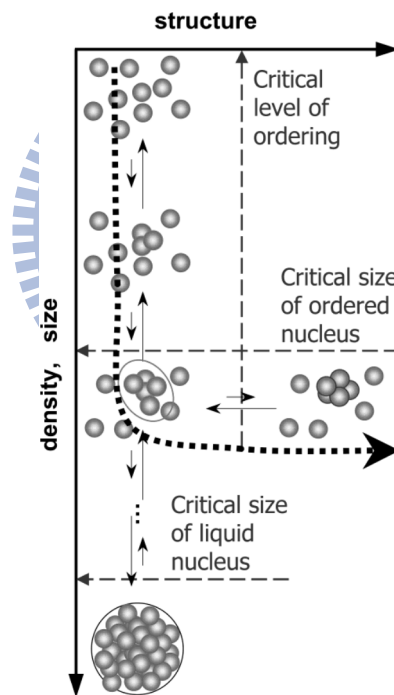
Fig. 1.3 Schematic illustration of the formation of ordered crystalline nuclei as a result of the superposition of a density and a structure fluctuations [20].

1.3 Light-induced crystallization

Light-induced crystallization can be realized with various light sources through different mechanisms such as photochemical and nonphotochemical (or photophysical) processes. The used light source can be Xe lamp, continuous wave laser or pulse laser at different wavelengths ranged from UV region to NIR region.

1.3.1 Photochemical reaction-induced nucleation

Okutsu et al. have reported photochemical reaction-induced nucleation of anthracene [21], hen egg-white lysozyme (HEWL) [22], thaumatin [23], and ribonuclease A (RNaseA) [24]. In the lysozyme crystallization experiment, they exposed UV light (wavelength; 280, 300 and 400 nm) from Xe short arc lamp (wavelength; 200-800 nm, USHIO UXL-300D) to
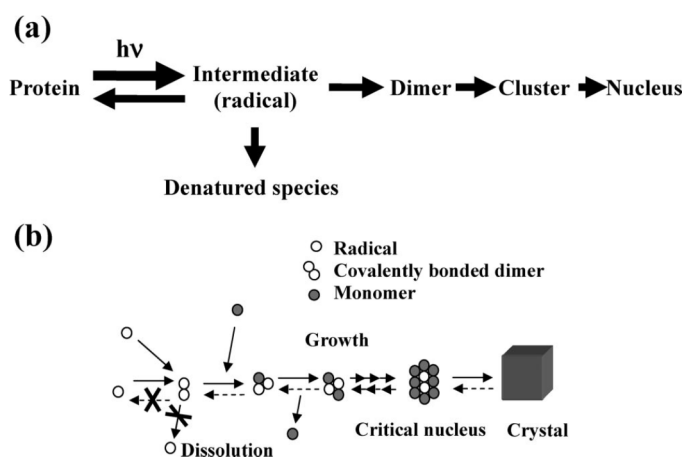
Fig. 1.4 (a) Mechanism of the photochemically induced nucleation of lysozyme (b) enhancement of protein crystallization by a photochemical reaction [22].

supersaturated but metastable lysozyme solution and produced photochemical intermediate (Fig. 1.4). Since the photoproduct has lower solubility in mother solution, it works as a nucleus and triggers crystallization eventually [22]. Okutsu et al. gave a representative demonstration of photochemical reaction-induced nucleation. However, it is not known for sure how radical formation affects the purity of the obtained protein crystal.

1.3.2 Kerr effect-induced nucleation

Garetz et al. discovered that intense nanosecond NIR laser pulses (pulse duration; 20 ns, repetition rate; 10 Hz, wavelength; 1.06 μm) can induce nucleation of urea solution in 1996. This phenomenon was named as nonphotochemical laser-induced nucleation (NPLIN). Because it was observed that the initially forming needle-shaped crystals tend to be aligned parallel to the electric field vector of the light, they proposed that the electric field-induced realignment of urea molecules results in cluster formation and this mechanism is known as the optical Kerr effect [25]. Nucleation of glycine [26] was also demonstrated, and the polymorph of glycine was controlled by changing polarization of laser beam [27] or by additionally applying strong DC electric field to enhance the optical Kerr effect [28].

1.3.3 Laser trapping crystallization

Continuous wave (CW) laser-induced crystallization has been developed very fast recently. Fig. 1.5 shows the principle of laser trapping. When a highly focused laser beam passes through sphere-like medium with a greater refractive index from surrounding, the sphere-like medium acts like a weak positive lens and it will be moved toward the focal point by a substantial net backward trapping force [29]. In laser trapping crystallization, tightly focused CW NIR laser beam is employed to gather molecules or clusters, forming a high concentration area at the focal spot, where the nucleation is eventually achieved. Since laser trapping is actually a dynamic process against diffusion of trapped molecules or clusters from the focal spot, in order to reach stable laser trapping condition, laser irradiation at a certain point for a period of time is necessary. Therefore, selecting laser wavelength at which both of solvent and solute have merely no absorption is quite important. Photons at NIR wavelength
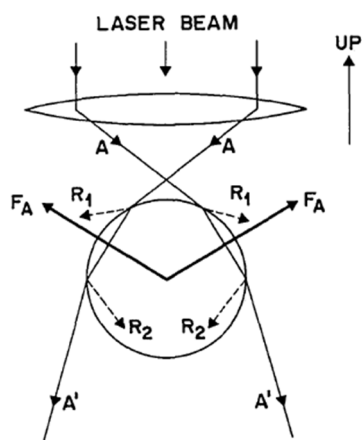
Fig. 1.5 Diagram showing the ray optics of a spherical Mie particle trapped in water by the highly convergent light of a single-beam gradient force trap [29].

have lower energy and can be less absorbed by biological molecules or systems. However, water as a common solvent is not applicable since it has vibrational absorption over 1000 nm [30]. The absorption of water generates a serious problem in temperature elevation which increases the solubility of solution, and crystallization becomes more difficult. In order to solve this problem, it is necessary to replace water with deuterated water (heavy water) as solvent in this crystallization method.

Sugiyama et al. has firstly demonstrated crystallization of glycine by an intense focused CW-YVO$_4$ laser beam (wavelength; 1064 nm) at the air/solution interface. It was observable by a CCD camera that the glycine crystal grew from focus to a certain size within a few seconds [31]. Furthermore, Rungsimanon et al. have investigated the method to control glycine phase by tuning laser power. It was found that the competing result between photon pressure and temperature elevation at a certain high laser power led to the probability increase to find γ-polymorph glycine crystal, which is not available under ambient conditions [32]. On the other hand, Yuyama et al. have demonstrated the preparation of a millimeter-scale dense liquid droplet of glycine induced by laser trapping effect. After focusing a CW NIR laser beam at the glass/solution interface of a thin film of its supersaturated heavy water solution and forming the droplet, they found that crystallization starts immediately just after the focal position is shifted to the air/solution interface. It is considered that the droplet formation is

possibly the early stage of the multistep crystallization process and plays an important role in

photon pressure-induced crystallization of glycine [33].

1.3.4 Molecular assembling induced by optical trapping

Tsuboi et al. reported that the aggregation of lysozyme as nucleus induced by optical

trapping in solution can trigger nucleation [34]. They also observed the assembling of amino

acids (glycine, proline, serine and alanine) induced by laser trapping in solution, and

considered that the observed glycine assembling may be experimentally verified as a

precursor for the crystal nucleus by Sugiyama et al. [35]. The differences between inducing

molecular aggregation as nucleus and forming a local high concentration area by trapping

laser are the focal position and the necessary time for observation. Molecular assembling is

induced in solution and takes several hours for observation, whereas laser trapping

crystallization can only be achieved at the air/solution interface and the crystal grows within

several seconds.

1.3.5 Femtosecond laser-induced crystallization

Femtosecond laser-induced crystallization of HEWL was firstly demonstrated in 2003 by

Hosokawa et al. [10]. Besides, urea [12], DAST (4-(dimethylamino)-N-methyl-4-stilbazolium

tosylate) [11], anthracene [13] and glucose isomerase (GI) [36] crystallizations were also

reported in following years. The mechanism will be introduced in detail in Chapter 2.

1.4 Motivation

In this work, we have focused on femtosecond laser-induced crystallization and tried to

clarify how laser parameters inclusive of pulse energy, repetition rate, focal position and

exposure time affect the crystallization probability, crystal morphology and crystalline phase.

Firstly, we demonstrated glycine crystallization since glycine crystal shows several

polymorphs and is well-studied in the field of crystal chemistry [14]. Then we applied our

obtained results to lysozyme crystallization since lysozyme is also a representative protein in

protein crystallography [19]. It is expected to sharpen present crystallization techniques with

optimizing laser parameters and simultaneously establish a remarkable milestone to study

molecular dynamics of femtosecond laser-induced crystallization under appropriate

conditions.

Chapter 2

Principle

The mechanism of femtosecond laser-induced crystallization is completely different from other methods because only this technique triggers nucleation by multiphoton absorption of solvent leading to optical breakdown and is less related with solute. Firstly, principle of multiphoton absorption is explained with its schematic illustration in Fig. 2.1. Since the energy of a single photon is not enough to excite a molecule from the ground state to a higher electronic state, the molecule can be excited only by absorbing more than one photons simultaneously and the energy difference between the two states is equal to the sum of the energy of the photons. Figure 2.2 reveals that water has much higher absorption in UV region due to electronic transition than in visible and NIR region due to vibrational overtone absorption [37], so it supports that water molecule are excited by photons at 800 nm through multiphoton absorption.

By focusing intense laser into water, multiphoton absorption of water occurs, and leads to optical breakdown of water giving vigorous evaporation if the superheated condition is satisfied. When the rate of volumetric energy deposition provided by laser irradiation is more

rapid than the rate of energy consumed by vaporization and normal boiling, the liquid water is

driven to a metastable superheated state. The liquid can remain metastable until the spinodal

temperature is reached. By viewing a plot of the Gibbs free energy versus specific volume at

ambient pressure as shown in Fig. 2.3, unique features of the spinodal temperature can be

appreciated.   At the spinodal temperature, the equilibrium between saturated liquid state and

saturated vapor state becomes extremely unstable, so the liquid undergoes spinodal

decomposition, a spontaneous process by which a thermodynamically unstable liquid relaxes

toward equilibrium. The superheated liquid transits to the vapor phase via spinodal

decomposition spontaneously. The generated vapor bubbles grow with increasing temperature,

and eventually stop growing and collapse at the maximum spinodal temperature just below

the critical temperature [38].
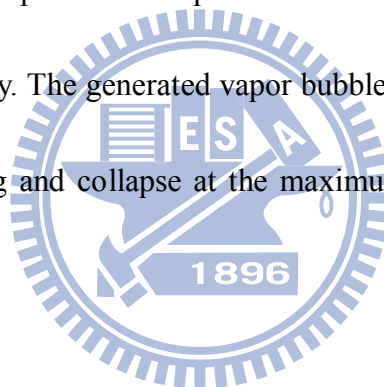
Although optical breakdown can be achieved in various common solvents such as water,

deuterated water and some organic solvents, water is still chosen as the best solvent for

crystallization in this study since water is easier to be obtained with much less cost, is more

environmentally friendly and always plays an important role in biological systems. Different

from laser trapping crystallization method in which deuterated water has been used as solvent

to prevent from temperature elevation induced by continual 1064 nm CW laser irradiation, it

is regarded as a great advantage that water can be used directly in femtosecond laser-induced
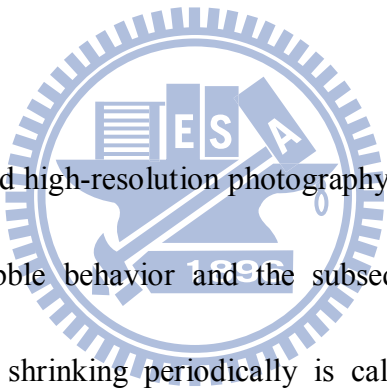
crystallization. Moreover, the wavelength of femtosecond laser can be adjusted to 800 nm at which it is well-known that neither water nor biological molecules such as amino acids and proteins have strong vibrational overtone absorption. Therefore, femtosecond laser is regarded as an appropriate light source to deal with biological molecules or systems such as proteins, cells and tissues which usually contains large amount of water and has been widely applied [30].

When an intense femtosecond laser light is focused into water, multiphoton absorption of water induces nonlinear phenomena such as shockwaves, cavitation bubbles, and jet flow formations in water (Fig. 2.5) [5]. These nonlinear phenomena were also described as laser tsunami. A real image of optical breakdown of water was shown in Fig. 2.6 while it was induced by picosecond laser irradiation but not femtosecond laser irradiation. Trace of shock wave propagation and cavitation bubble generation can be clearly observed, and the spatial and temporal intensity decays of local transient pressure induced by shock wave were also recorded as shown in Fig. 2.7 and Fig. 2.8, respectively [39].

Lord Rayleigh discussed the collapse behavior of a spherical cavity in a homogeneous incompressible liquid and established a mathematical model to calculate time-dependent radii in 1917 [40]. After that, Juhasz et al. reported time-resolved observations of shock waves and

cavitation bubbles generated by femtosecond laser pulses, and compared the results with

theoretical calculations derived by L. Rayleigh (Fig. 2.9) [41].

Laser tsunami as local physical perturbations in supersaturated solutions has been

utilized to trigger the nucleation by increasing local concentration as shown in Fig. 2.10

[10-13, 36]. Since the duration time of femtosecond laser pulse is too short to accumulate heat

near focal point, it is considered that femtosecond laser-induced crystallization takes place

under constant temperature.

Recently, high-speed and high-resolution photography have also been used to investigate

laser-induced cavitation bubble behavior and the subsequent nucleation of crystals. The

bubble size expanding and shrinking periodically is called Rayleigh bubble. In order to

discuss the importance of Rayleigh bubble to crystallization, Murai et al. increased the

viscosity of lysozyme solution by adding agarose gel against protein diffusion from the focal

point and recorded the conformation change of bubbles. They successfully observed the

formation of locally high concentration region induced by bubble conformation change

leading to elevate crystallization probability around the surface of bubble [42, 43]. Nakamura

et al. previously observed film-like crystal formation of anthrathene along with the bubble

surface when a single femtosecond laser pulse was focused in solution (Fig. 2.11) [13].

Another supporting evidence is that Soare et al. observed ring-shaped optical disturbance which originates from refractive index change induced by crystal nuclei formation after collapse of cavitation bubble [44].
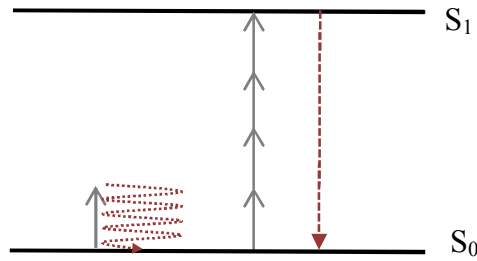
Fig. 2.1 Schematic illustration of multiphoton absorption.
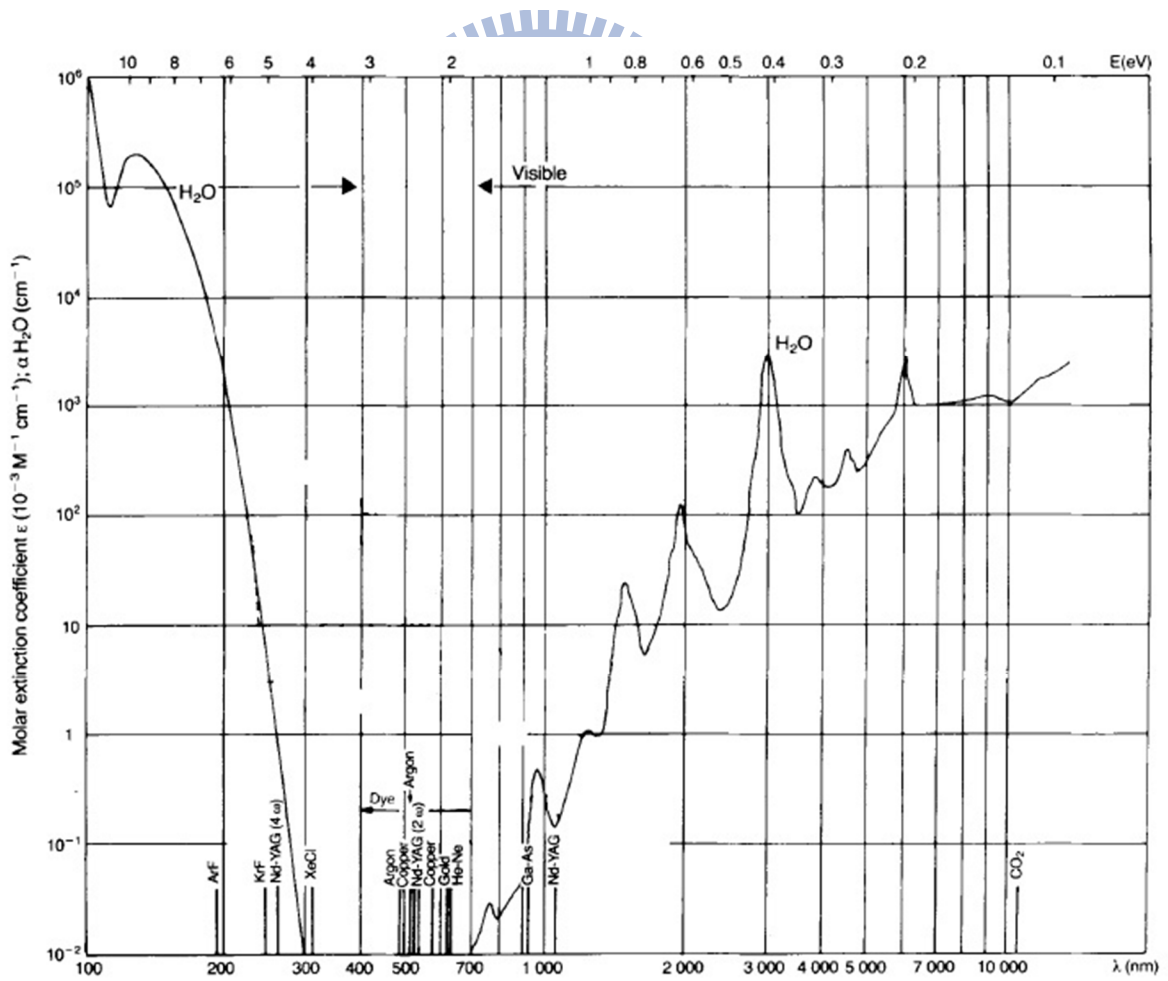
Fig. 2.2 Absorption coefficient spectrum of water, together with the wavelength positions of the most widely used lasers [36].
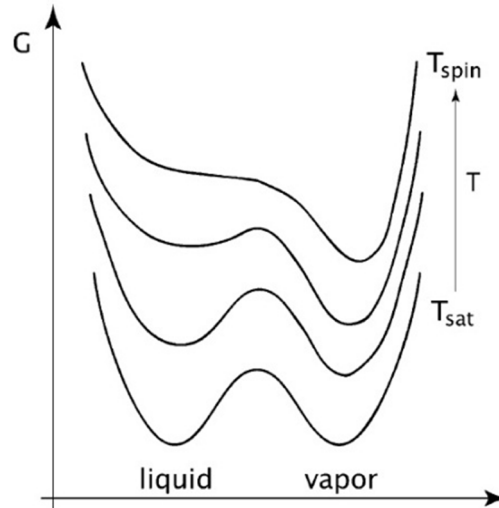
Fig. 2.3 Gibbs free energy versus specific volume of a pure substance for several temperatures starting at the saturation temperature, T_{sat}, where the liquid and gaseous states are in equilibrium, up to the spinodal temperature, T_{spin}. Note that the local minimum corresponding to the liquid phase disappears at the spinodal temperature, effectively forcing conversion of the substance to the vapor phase [37].
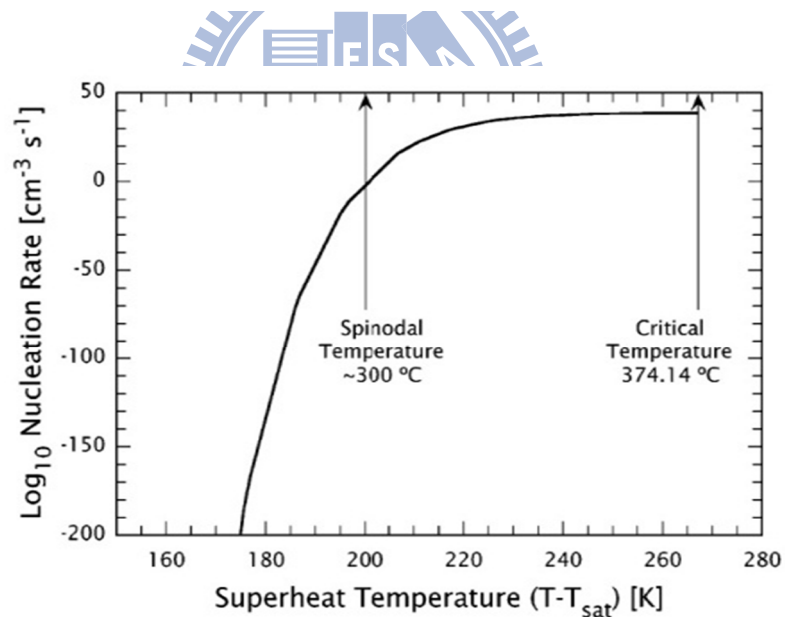
Fig. 2.4 Variation of vapor bubble nucleation rate with superheat temperature [37].
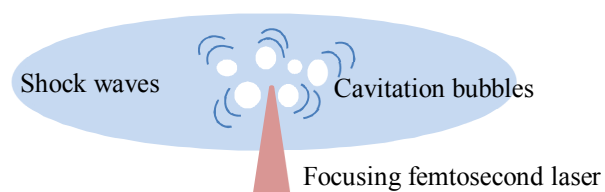
Fig. 2.5 Schematic illustration of laser tsunami in water.
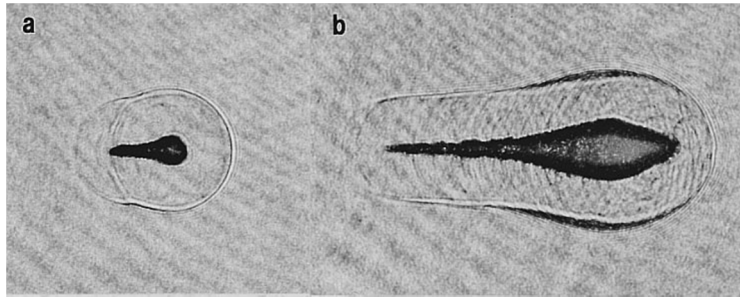
Fig. 2.6 Plasma, shock wave, and cavitation bubble produced by Nd:YAG laser pulses of different duration and energy: (a) 30 ps, 50 µJ; (b) 30 ps,1 mJ. All pictures were taken 44 ns after the optical breakdown [38].
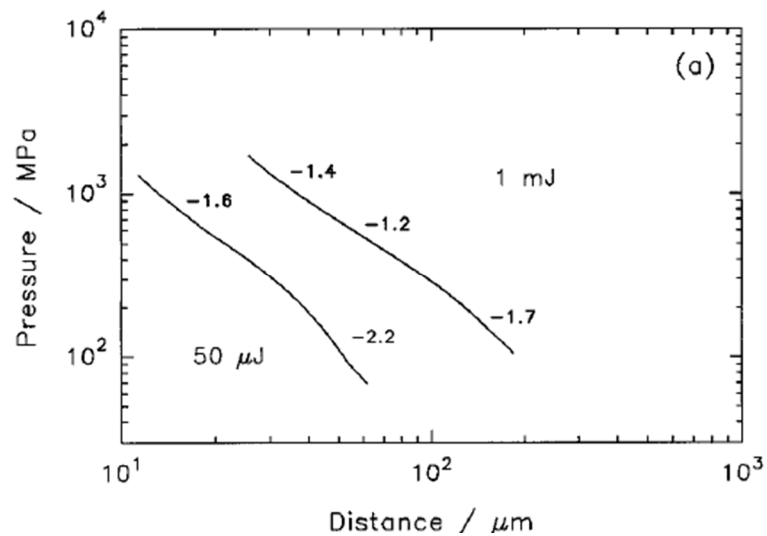
Fig. 2.7 Experimentally determined shock wave pressure after pulses of 30 ps duration with 50 µJ and 1 mJ energy. The numbers indicate the local slope of the curves [38].
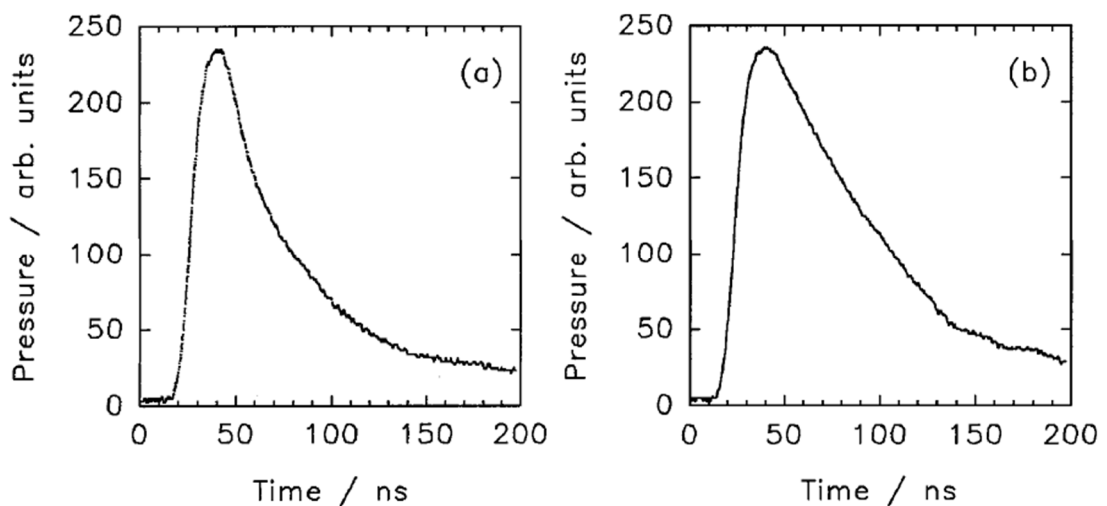
Fig. 2.8 Hydrophone signals measured at a distance of 10 mm from the emission center of the shock waves. The respective values of laser pulse duration and energy are (a) 30 ps, 50 µJ; (b) 30 ps, 1 mJ [38].
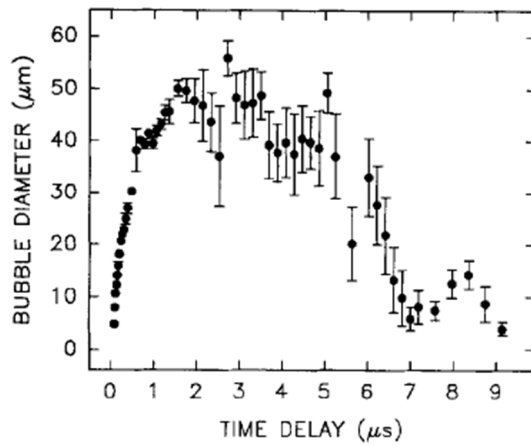
Fig. 2.9 The diameter of the cavitation bubble in water as a function of time. The laser fluence is 9 J/cm^2 [40].
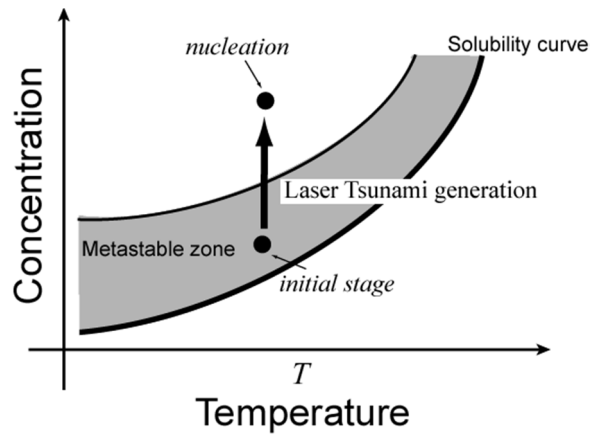
Fig. 2.10 Spatially limited transient pressure generated by femtosecond laser can induce molecular nucleation in supersaturated solution.
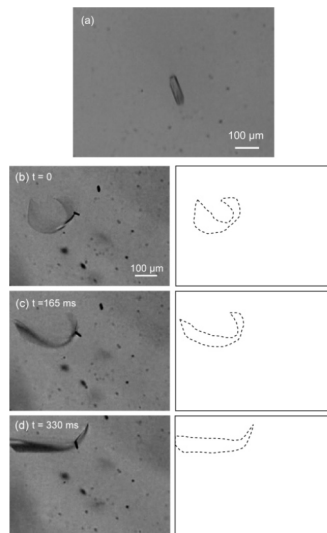
Fig. 2.11 Microscopic images of generated anthracene crystals at a pulse energy of 6.7 µJ/pulse (a) and a growth process of a bending film-like crystal created at the surface of a large laser-induced bubble at a pulse energy of 16.5 µJ/pulse (b-d) [13].

Chapter 3

Experiment

3.1 Experimental setup

3.1.1 Femtosecond laser light source

Amplified Ti:sapphire femtosecond laser which is composed of a mode-locked Ti:sapphire laser and Chirp Pulse Amplification (CPA) was used as the light source in this study. A mode-locked Ti:sapphire laser light (wavelength; 700-900 nm, repetition rate; 80 MHz, pulse duration; 160 fs, Tsunami, Spectra Physics) was generated when it was pumped by a continuous wave solid-state visible laser (wavelength; 532 nm, Millenia Pro, Spectra Physics) at about 7 W and was controlled by an electronics module (Model 3955, Spectra Physics). A prism sequence and a slit were used for dispersion control and wavelength selection, respectively. Spectral information of the output laser light was provided by a fiber optic spectrometer (USB4000, Ocean Optics). After full width at half maximum (FWHM) of the spectrum and central wavelength of the laser light were determined to be about 12 nm and 800 nm simultaneously, the laser light was amplified by a Ti:sapphire regenerative amplifier system (Spitfire Pro, Spectra Physics).

Since self-focusing, a nonlinear optical effect in which an intense light beam modifies the refractive index of the material it is passing through, takes place and causes permanent damage to the Ti:sapphire crystal, it is necessary to limit the peak power of a pulse below 10 GW/cm^2 during amplification. Therefore, CPA was applied to the system to amplify pulse beyond the peak power and to keep the power density far below the damage threshold of the crystal. CPA was accomplished in the following three steps (Fig. 3.5). The first step stretched the seed pulse supplied from a stable and mode-locked femtosecond laser to about 10^4 times. Stretching the pulse reduces its peak energy, which greatly reduces the probability of damage to the crystal at the same time. The second step amplified the stretched pulse by passing it through the Ti:sapphire regenerative amplifier. Finally, a set of dispersive optics was used to recompress the stretched, amplified pulse as close as possible to its original duration and high peak power compressed pulse was generated.
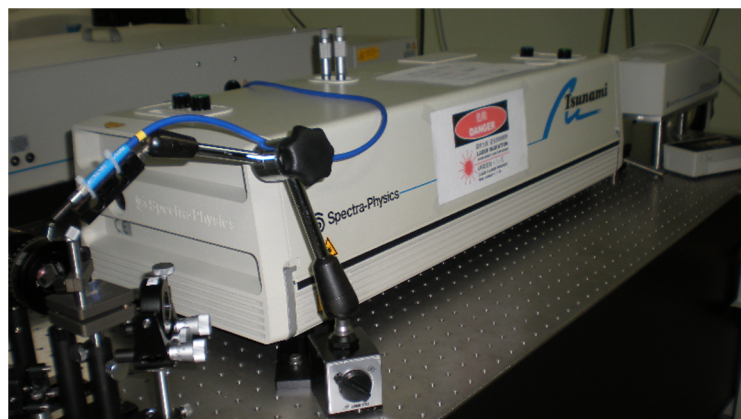
Fig. 3.1 Picture of mode-locked Ti:sapphire laser, Tsunami.
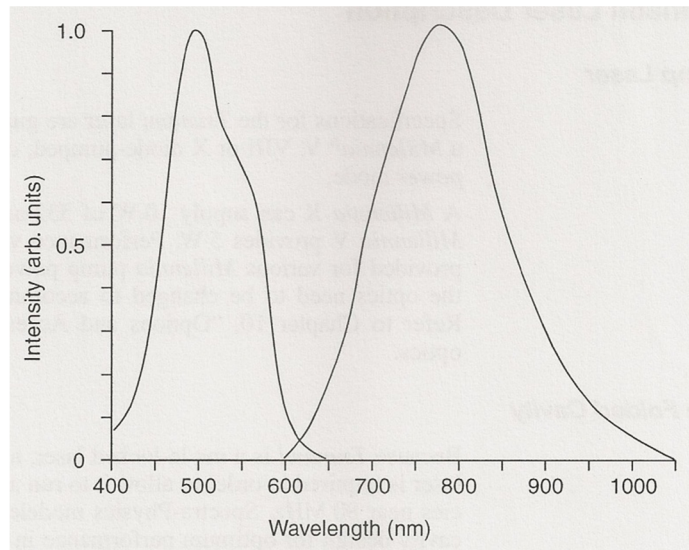
Fig. 3.2 Absorption and emission spectra of Ti:sapphire.
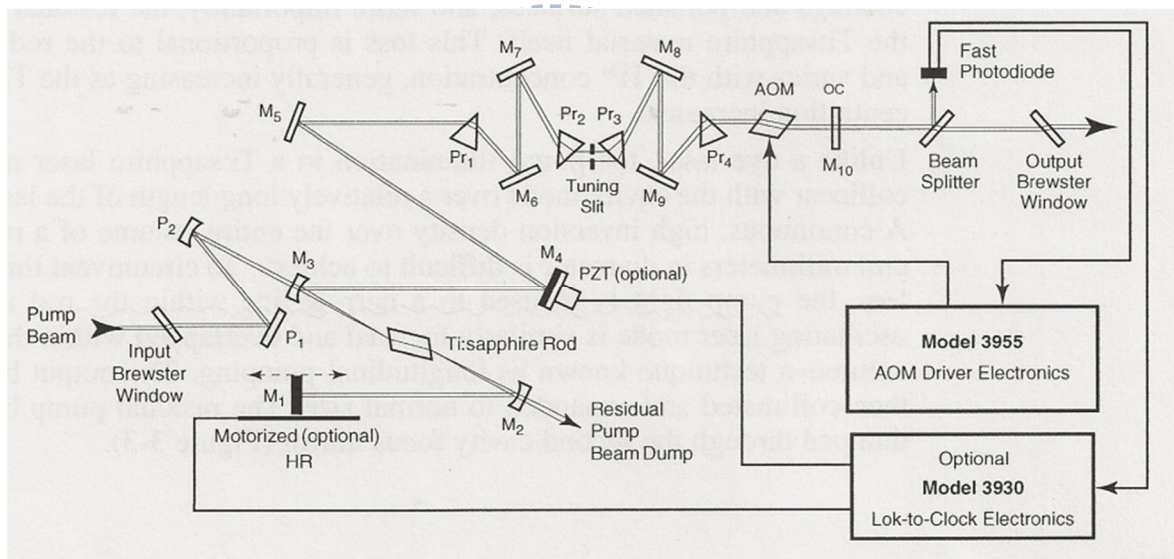
Fig. 3.3 The mode-locking principle in Tsunami.

Fig. 3.4 Picture of Ti:sapphire regenerative amplifier system, Spitfire Pro.
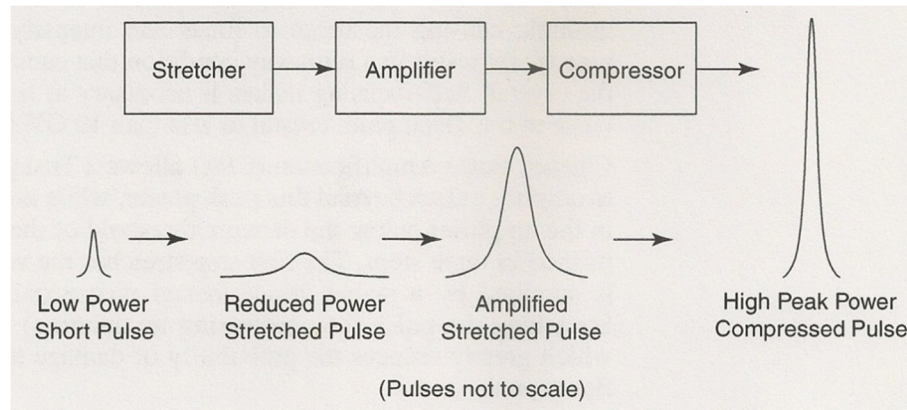
Fig. 3.5 The schematic illustration of CPA principle.

3.1.2 Experimental setup

The experimental setup is shown in Fig. 3.6. Linearly polarized femtosecond laser pulses from femtosecond laser (wavelength; 800 nm, pulse duration; 160 fs, Spitfire Pro, Spectra Physics) were introduced to an inverted microscope (IX-71, Olympus) through an objective lens (10×, N.A. 0.25, PlanN, Olympus). Pulse energy was adjusted by using a half-wave plate, a polarizing beam splitter, and a variable neutral density filter, and was measured after an objective lens by energy meter (842-PE, Spectra Physics). The repetition rate of femtosecond laser pulse train was controlled by a Pockels Cell. The crystal formation and crystal morphology were observed with a digital CCD camera (CV-S3200N, JAI) attached to the microscope. All the experiments were carried out at room temperature (22℃).
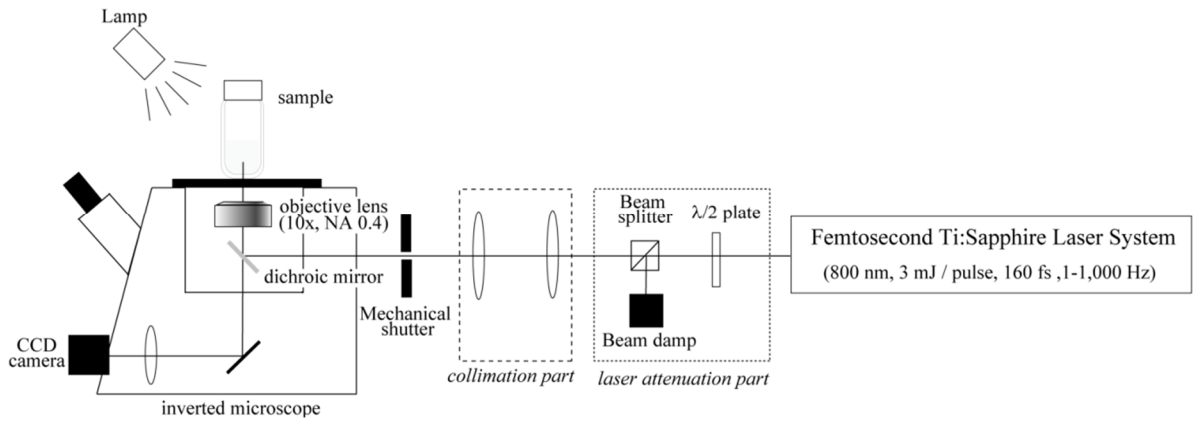
Fig. 3.6 Laser light source and microscopic system for crystallization.

Fig. 3.7 Picture of inverted microscope and other attachments.
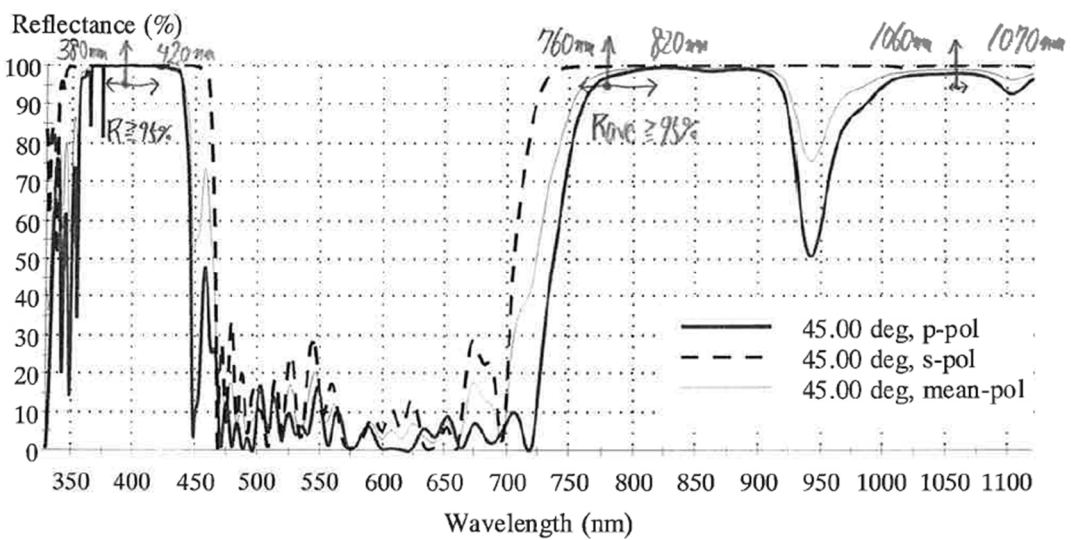
Fig. 3.8 Reflectance spectrum of the dichroic mirror used in the inverted microscope
[45].
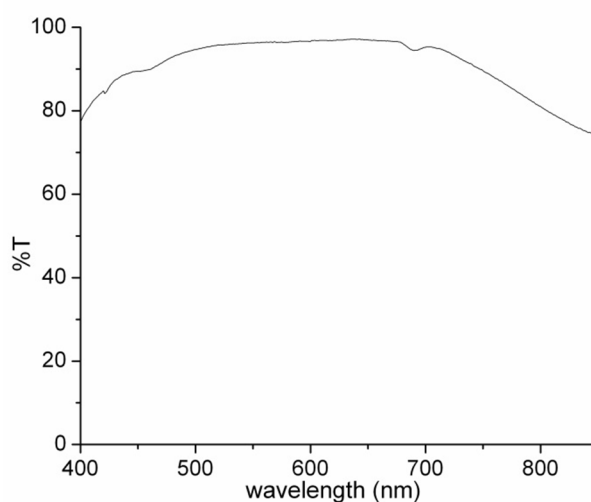
Fig. 3.9 Transmittance spectrum of the objective lens used in the inverted microscope.

3.1.3 Confocal Raman microspectroscopic system

Confocal Raman microspectroscopic measurement was performed to characterize the crystalline phase of obtained crystals with a confocal unit coupled optical inverted microscope (FV300, Olympus). Raman signals were obtained by exposing 532 nm DPSS laser beam (40 mW, JLW-532-200, SLOC) through a line filter and an objective lens (10×, N.A. 0.25, PlanN, Olympus) to the crystals placed on the microscope stage, and were recorded by a CCD camera combined with polychromator with a 150 gr/mm grating (polychromator; SpectraPro 2300i, CCD camera; PIXIS400, Princeton instruments) after passing through a confocal aperture (500 μm). By fast laser scanning a certain detecting two-dimensional area of the obtained crystals with a Galvano mirror unit, Raman images were also recorded.

3.1.4 Surface tension measurement

Surface tension is a property of a liquid surface that allows it to resist an external force. In the bulk of the liquid, each molecule is pulled equally in every direction by neighboring liquid molecules, resulting in a net force of zero. The molecules at the surface do not have other molecules on all sides of them and therefore are pulled inwards. This creates some internal pressure and forces liquid surfaces to contract to the minimal area. Similar to surface tension, molecular adsorption is related to surface energy. In a bulk material, all the bonding requirements of the constituent molecules of the material are filled. The molecules on the surface experience a bonding deficiency because of the dissymmetric surrounding. Therefore, it is energetically favorable for them to attract adsorbates.
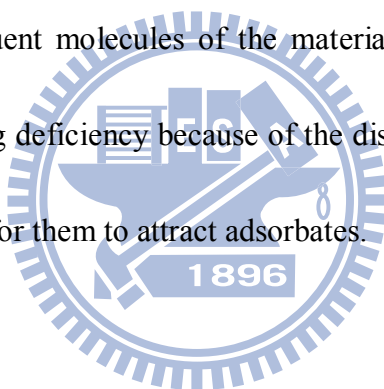
The du Noüy ring method, a relatively simple method with much higher precision proposed by the French physicist Pierre Lecomte du Noüy in 1925 [46], is applied to measure surface tension of sample solution here. As Fig. 3.10 shows, a hanging and relatively immobile thin platinum ring (diameter of wire 2r; 0.3 mm, diameter of ring 2R; 13.5 mm, Narika) connected with an electronic balance (minimum weight; 0.1 mg, CP124S, Sartorius) from the bottom is submersed in a solution on a stage, and then the height of the stage is slowly decreased at a constant speed. As the ring is almost pulled out of the liquid, the maximum force F required is precisely measured and can determine the surface tension γ of

the liquid. The following is the formula:

$$\gamma = \frac{F}{4\pi R} \quad \text{...(3.1)}$$

W. D. Harkins and H. F. Jordan considered that the shape of liquid film is strongly dependent on the radius of the ring, the radius of the wire, the density of the solution and the surface tension, compared with the maximum force F obtained by both the ring method and the capillary method (Fig. 3.11 [47]), and suggested that the obtained surface tension γ with ring method should be modified by a correction factor $f(\text{R}^3/\text{V}, \text{R/r})$ [48]. Therefore, the real surface tension is shown as the following formula:

$$\gamma = \frac{F}{4\pi R} \, f\left(\frac{R^3}{V}, \frac{R}{V}\right) \quad \text{...(3.2)}$$
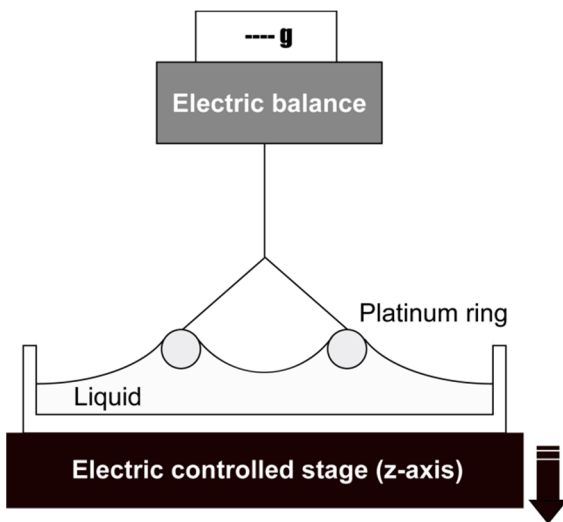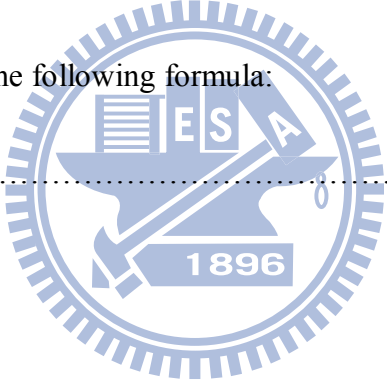
Fig. 3.10 Illustration of the du Noüy ring method.
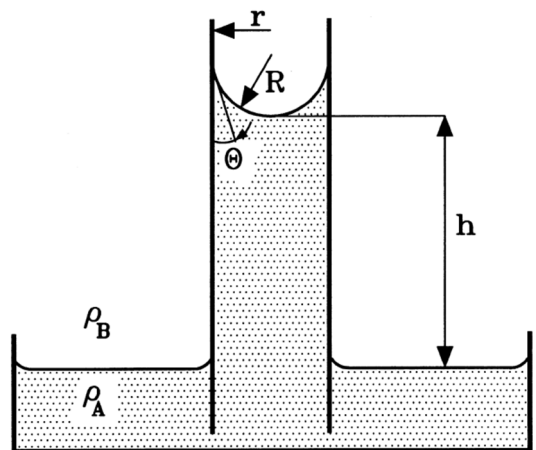
Fig. 3.11 Illustration of the capillary method [47].

3.1.5 X-ray diffraction

X-rays as electromagnetic waves are diffracted by a crystal in many directions. Following Bragg's law, constructive interference of X-rays scattered by a crystal occurs in a few specific directions. These diffraction data inclusive of intensities and phases in reciprocal space can derive the dimensions of the unit cell and the molecular structure in real space through Fourier transform. In fact, X-rays are mainly scattered by the electrons but not nuclei in the atoms. Therefore, a primitive data of electron density distribution is firstly obtained from the diffraction pattern. After repeating fitting the atomic model and refinement again and again, molecular structure at atomic scale can be reconstructed [15].
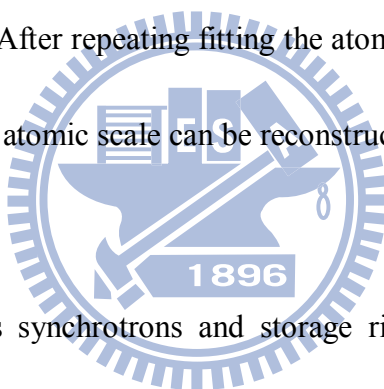
Particle accelerators as synchrotrons and storage rings are the most powerful X-ray sources, and they are profitably used by protein X-ray crystallographer for data collection on weakly diffracting specimens such as very tiny crystals or crystals with extremely large unit cells. Synchrotrons are facility for circulating electrically charged particles at nearly the speed of light. The particles are injected into the storage ring directly from a linear accelerator or through a booster synchrotron. When the particle beam changes direction, the electrons or positrons are accelerated toward the center of the ring, emit electromagnetic radiation, and consequently lose energy. This energy loss is compensated by a radiofrequency input at each cycle. The main advantage of synchrotron radiation for X-ray diffraction is its high intensity

which is two orders of magnitude stronger than a conventional X-ray tube. Another advantage

is the low divergence of the beam resulting in sharper diffraction spots [15].

3.2 Sample preparation

3.2.1 Supersaturated glycine aqueous solution

Glycine (99.0%, Lot. No. LTF4344, Wako Pure Chemical) in the form of white powder

was used without further purification. Deionized water as solvent was filtrated with a syringe

filter (pore size; 0.22 μm, SLGV 013 SL, Millipore) before dissolving glycine. 1.5 ml glass

bottle (Nichiden Rika Glass) (Fig. 3.12) as container was cleaned by plasma cleaner (ATTO,

diener electronic). 0.5 ml of supersaturated glycine aqueous solution was prepared at 3.0 M,

3.5 M and 4.0 M (C_{sat}= 3.0 M [49]) in glass bottle with cap screwed on. The solution was

slowly heated up from room temperature to 60℃ in water bath at heating rate 5℃ per hour

until glycine was completely dissolved, and was cooled down to room temperature

spontaneously.

Fig. 3.12 Picture of 1.5 ml glass bottle
with 0.5 ml glycine solution inside.

3.2.2 Supersaturated lysozyme aqueous solution

3.2.2.1 Acetic acid-sodium acetate buffer aqueous solution

Filtrated deionized water was also used as solvent here. 200 mM acetic acid solution was prepared by adding 120 µl acetic acid (99.8%, Sigma-Aldrich) into 10 ml water. On the other hand, 200 mM sodium acetate solution was prepared by adding 0.164 g sodium acetate (Sigma-Aldrich) into 10 ml water. 2.9 ml acidic solution and 2.1 ml basic solution are mixed and diluted with 5 ml water. Finally, the obtained solution was 100 mM acetic acid-sodium acetate aqueous solution used as buffer solution and its pH was about 4.5 measured by pH meter (pHi 510, Beckman Coulter) [50].
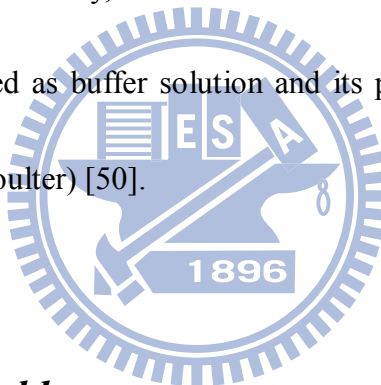
3.2.2.2 Supersaturated lysozyme aqueous solution

Lysozyme from egg white or hen egg white lysozyme (HEWL) (for Biochemistry, Lot. No. PEK3768, Wako Pure Chemical) in the form of white powder was used without further purification. Supersaturated lysozyme solution was prepared with buffer solution at 40 mg/ml at room temperature. After lysozyme was completely dissolved in buffer solution, sodium chloride (>99.9%, FSA Laboratory Supplies) as a crystallization agent was added to slightly decrease protein solubility. The pH of prepared solution was not much changed after lysozyme powder and salt were added into buffer solution. Lysozyme is active and has been

crystallized successfully at pH around 4.5 [19, 51]. The solution was dropped into wells

fabricated on a plastic crystallization plate (VDX48 Plate with sealant, Hampton) (Fig. 3.13)

with 50 µl in each well sealed with glass coverslip (Matsunami).

Fig. 3.13 Picture of crystallization plate.

Chapter 4

Glycine Crystallization

4.1 Introduction

It is well-known that protein is a biological macromolecule composed of 20 common amino acids. Glycine, NH_2CH_2COOH, is a common amino acid with lowest molecular weight and simplest structure (Fig. 4.1), and has been repeatedly studied in the field of crystal chemistry.
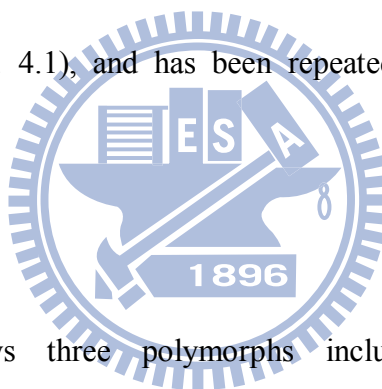
Glycine crystal shows three polymorphs inclusive of two monoclinic with centrosymmetric space groups (α, s.gr. $P2_1/n$, and β, s.gr. $P2_1$) and one trigonal with non-centrosymmetric space group (γ, s.gr. $P3_1$) [52-54]. The shape difference between α- and γ-polymorph glycine crystals can be clearly distinguished in Fig. 4.2. Many groups have employed glycine as a standard sample to laser-induced crystallization methods. It can be
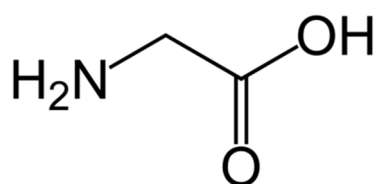
Fig. 4.1 The chemical structure of glycine.

expected that the detailed study on femtosecond laser-induced glycine crystallization will be more helpful to understand the laser parameters effect by comparison with such previous work.

Usually, commercially available glycine powder contains mixture of α- and γ-polymorphs. The polymorph content obtained from different chemical companies or even just different packages of the same company ranges from α with admixture of γ to γ with admixture of α. γ-polymorph crystal is the most thermodynamically stable among these three polymorphs, but spontaneous crystallization gives α-polymorph under almost every experimental condition. Crystal of γ-polymorph is preferentially obtained under relatively severe conditions such as using acid and base water solutions, using heavy water solution, and adding compounds that inhibit the growth of α-glycine like hexafluoravaline. However, based on our experimental result, it is still difficult to prepare γ-polymorph crystal under using

Fig. 4.2 The shapes of (a) α-polymorph and (b) γ-polymorph glycine crystals [14, 53].

heavy water as solvent. In fact, the success of crystallizing γ-polymorph seems to depend

much more on the presence of the seeds of this polymorph in the powder used for preparing a

saturated solution, than on the solvent used. To obtain β-polymorph crystal, ethanol should be

used to precipitate this form from a saturated water solution. However, a mixture of the α-

and the β-polymorphs can be always obtained [52, 54].

The transformations among these three polymorphs are very complicated [52]. Although

α-polymorph is quite stable at room temperature, it transforms to γ-polymorph after several

months. The transformation rate is highly dependent on the humidity of environment. High

humidity accelerates the transformation rate. β-polymorph prefers to transform to α- but not

γ-polymorph under high humidity but can be preserved well in dried environment.

β-polymorph also transforms to α-polymorph with heating below 100℃ or mechanical shocks

such as crush. γ-polymorph is quite stable at room temperature, but it transforms to

α-polymorph at 165℃. And reverse transformation does not take place immediately even after

γ-polymorph is cooled down to room temperature [14, 53].

4.2 Results

The possibilities of crystallization were recorded as crystallization probability here. The

crystallization probability defined here is the number of crystallized samples divided by the

total number of samples done at the same condition. Experiment was repeated 10 times under each condition. In order to confirm that the crystals are obtained by femtosecond laser irradiation rather than spontaneous crystallization, several blank samples under each condition were prepared for reference simultaneously.

4.2.1 Pulse energy dependence

Pulse energy dependence of glycine crystallization probability is shown in Fig. 4.3. Laser pulse train was focused at the solution/glass interface, which was actually about several tens
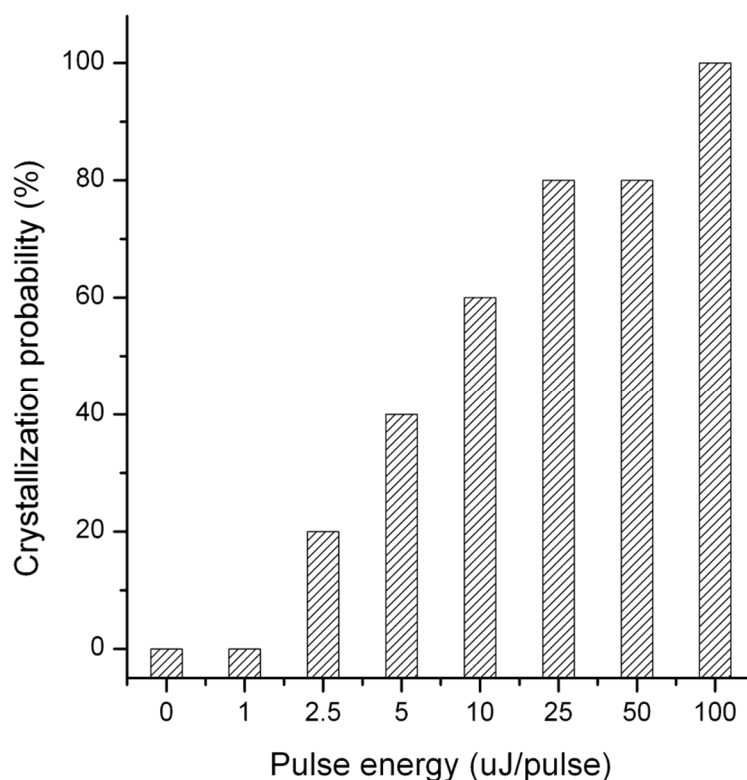
Fig. 4.3 Pulse energy (μJ/pulse) dependence on glycine crystallization probability (%). Repetition rate, exposure time, sample concentration and focal position are 1 kHz, 10 minutes, 4.0 M and several tens μm from the bottom of the bottle, respectively.

μm above the interface, to avoid laser ablation of glass. Cavitation bubble generation

threshold is confirmed by a CCD camera (Fig. 4.4). With increasing the pulse energy,

crystallization probability increased, while it showed a threshold of crystallization around 2.5

μJ/pulse, which was in good agreement with that of cavitation bubble generation.
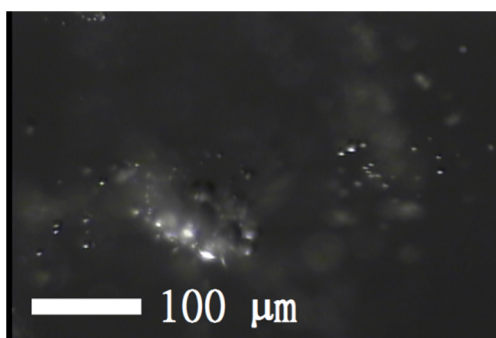
Fig. 4.4 The CCD image of cavitation bubble generation. When the pulse energy is 2.5 μJ per pulse, cavitation bubbles are generated around the focal point.

4.2.2 Repetition rate dependence

Crystallization probability and crystal morphology dependence on repetition rate of

irradiated femtosecond laser pulse train are recorded in Fig. 4.5. Pulse energy, irradiation time,

and focal position were fixed to 100 μJ per pulse, 10 minutes and at the solution/glass

interface, respectively. After waiting for several hours from femtosecond laser pulses

irradiation, we successfully obtained glycine crystals in the glass bottle.

It is found that the crystallization probability increased with the repetition rate and it

became saturated to 100 % above 250 Hz. On the contrary, at low repetition rate less than 5

Hz, crystals could not be obtained. In addition, it was confirmed that crystal morphology

exhibited a strong correlation with the repetition rate (Fig. 4.5 (b) and (c)). At lower repetition

rates, transparent single crystals with prismatic morphology floating on the solution were

obtained frequently. The size of the single crystals was roughly $5\times4\times3$ mm^3. Besides,

powder-like crystals were more likely to be observed at higher repetition rates. These

powder-like crystals are quite many, small, and uniform sized (mean size; $50\times20\times10$ μm^3).

Multiple crystals about 5-10 number with $2\times1\times1$ mm^3 were dominantly observed at the
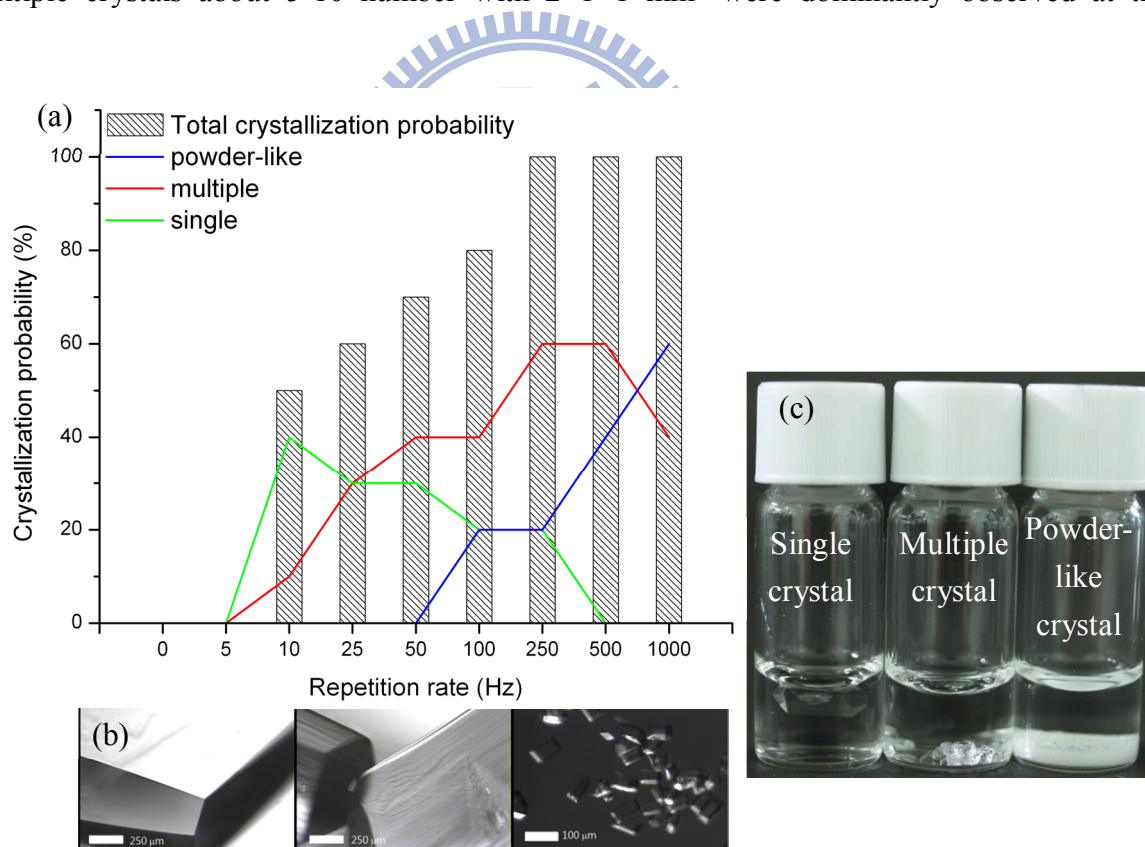
Fig. 4.5 (a) Crystallization probability (%) and crystal morphology dependence on repetition rate (Hz). (b) Images obtained from CCD camera. (c) Picture taken by general camera. Pulse energy, exposure time, sample concentration and focal position are 100 μJ per pulse, 10 minutes, 4.0 M and several tens μm from the bottom of the bottle, respectively.

middle rates around 50 Hz.

It is also found that crystal formation period was closely related to crystal morphology. In this experiment, single crystal formation took at least 3 to 4 days to be observed. However, the formation period was dramatically shortened as the size of crystal decreased. Powder-like crystal formation could be observed during pulse irradiation.

4.2.3 Focal position dependence

The result of focal position dependence is shown in Fig. 4.6. Pulse energy, irradiation time, and focal position were fixed to 100 μJ per pulse, 10 minutes and at the air/solution interface, respectively. Compared with the result of repetition rate dependence at the solution/glass interface, it was observed that the crystallization probability was significantly improved even at relatively low repetition rates such as 5 Hz and powder-like crystals were always obtained during laser irradiation when we irradiated the laser light at the air/solution interface.

In order to confirm the interface effect, the focal position was shifted from the solution/glass interface to the air/solution one with 1 mm step (Fig. 4.7). The solution thickness in the bottle was about 3 mm, so the crystallization probabilities were recorded at 4

focal positions with 1 mm interval. As the result, it is found that the crystallization probability

is improved upon both air/solution and glass/solution interfaces irradiation whereas the

probability is higher at the air/solution irradiation. In contrast to their interface irradiation, the
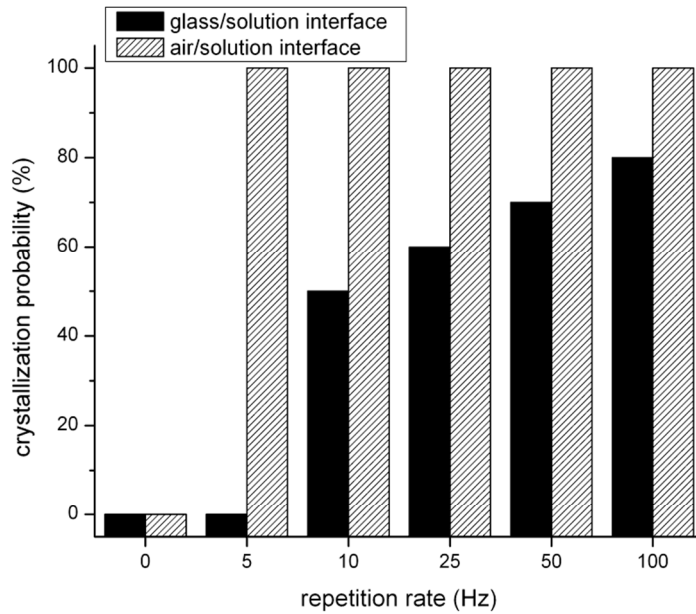
Fig. 4.6 The crystallization probability (%) depending on the repetition rate (Hz) at the air/solution interface or glass/solution interface. Pulse energy, exposure time and sample concentration are 100 μJ per pulse, 10 minutes and 4.0 M, respectively.
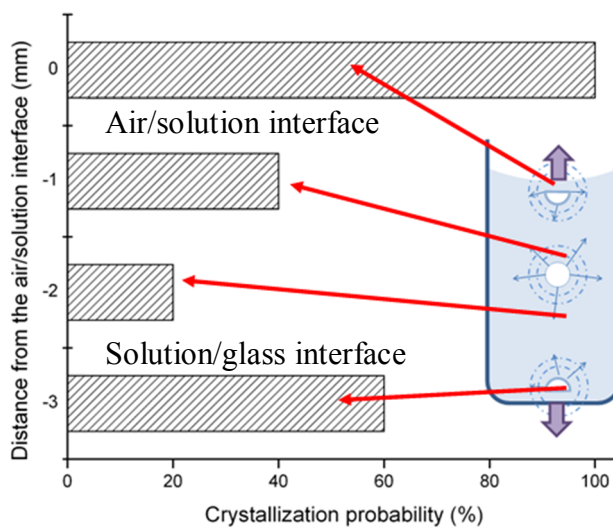
Fig. 4.7 The crystallization probability (%) depending on the distance from the air/solution interface (mm). Repetition rate, pulse energy, exposure time and sample concentration are 25 Hz, 100 μJ per pulse, 10 minutes and 4.0 M, respectively.

42

irradiation inside the solution suppressed the probability in spite of relatively higher probability at the position closer to air/solution interface. Therefore, we conclude that utilizing interface can improve crystallization probability in femtosecond laser induced crystallization and the irradiation at air/solution interface is more efficient.

4.2.4 Concentration dependence

From the view point of crystallography, it is well-known that the quality of the crystal in low supersaturated solution is much higher than that in highly supersaturated solution, which has been recognized in the conventional crystallization methods [31]. Therefore, it is expected to obtain crystals at relatively lower saturated concentration.
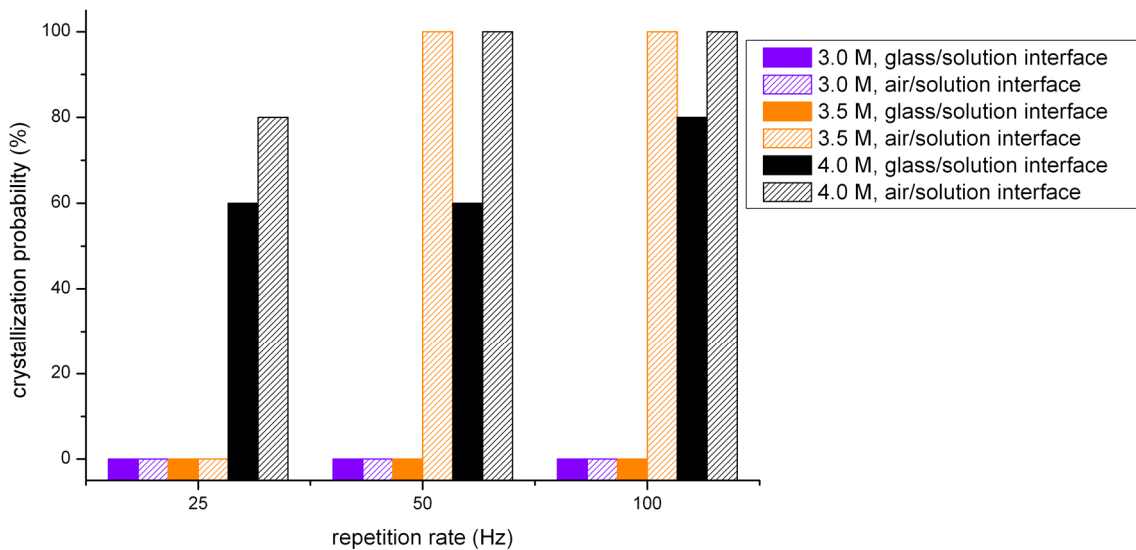
Fig. 4.8 The crystallization probability (%) depending on the repetition rate (Hz) at 3.0 M, 3.5 M and 4.0M. Repetition rate and exposure time are 50 µJ per pulse and 10 minutes, respectively.

Glycine solutions at lower supersaturated concentration and even saturated concentration

(C_{sat}=3.0 M) were irradiated by laser focused at the air/solution interface and the

solution/glass interface. Concentration dependence at three different repetition rates is

presented in Fig. 4.8. It is found that it is possible to get crystals even at lower concentration

(3.5 M) when we irradiated laser pulses at the air/solution interface at 50 and 100 Hz, and the

crystallization probability is apparently higher. However, it is difficult to form crystal when

we irradiated laser pulses at the solution/glass interface at the same repetition rates. Compared

with the case at saturated concentration (3.0 M), it is still difficult to crystallize at neither the

air/solution interface nor the solution/glass interface at even higher repetition rate such as 100

Hz.

4.2.5 Exposure time dependence

Since the crystallization probability reached such a high enough value when we

irradiated laser pulse at the air/solution interface, we tried to reduce the laser irradiation time.

It was expected to simplify the conditions and finally achieve single crystal formation by

single laser pulse, which is the simplest and the most ideal condition to study the molecular

dynamics of femtosecond laser-induced crystallization.

Consequently, needle-like crystals were more likely to be obtained at lower repetition

rate when the samples were irradiated with shorter exposure time. The crystal grew within several minutes just after laser irradiation. Hence, as the results of optimizing laser parameters based on our findings, we finally can create single crystal formation by single laser shot irradiation with 100 μJ to the air/solution interface with high probability about 10 %, and the same work cannot be achieved by irradiating only a single focused laser shot inside the solution under otherwise invariant conditions.
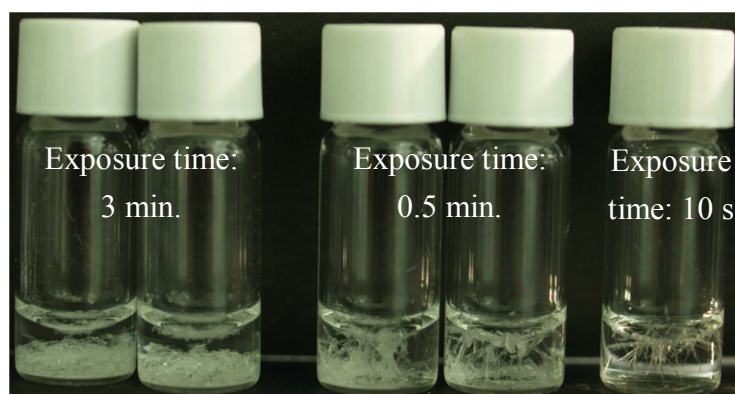
Fig. 4.9 The crystals obtained with different exposure times. Repetition rate, pulse energy, sample concentration and focal position are 5 Hz, 100 μJ per pulse, 4.0 M and air/solution interface, respectively.

4.2.6 Characterization

In order to characterize the crystalline phase and examine the purity of the obtained glycine crystals, Raman spectroscopic measurement, mass spectrometry analysis and X-ray analysis are used, respectively.

4.2.6.1 Confocal Raman microspectroscopic measurement

The crystalline phase of the obtained crystals was characterized by Raman spectroscopic measurement. The obtained crystals of different morphologies inclusive of single crystals, multiple crystals and powder-like crystals were taken out from the sample bottle, placed on a glass coverslip (Matsunami), and put on the microscope stage. Raman signals inclusive of spectra and images were recorded. As the result, all of the obtained crystals shows 1325 cm^{-1} peak in Raman spectrum and that peak is ascribed to α-form glycine crystal (Fig. 4.10 (b)) [55], which is the same polymorph as the glycine crystal obtained by spontaneous crystallization [52].
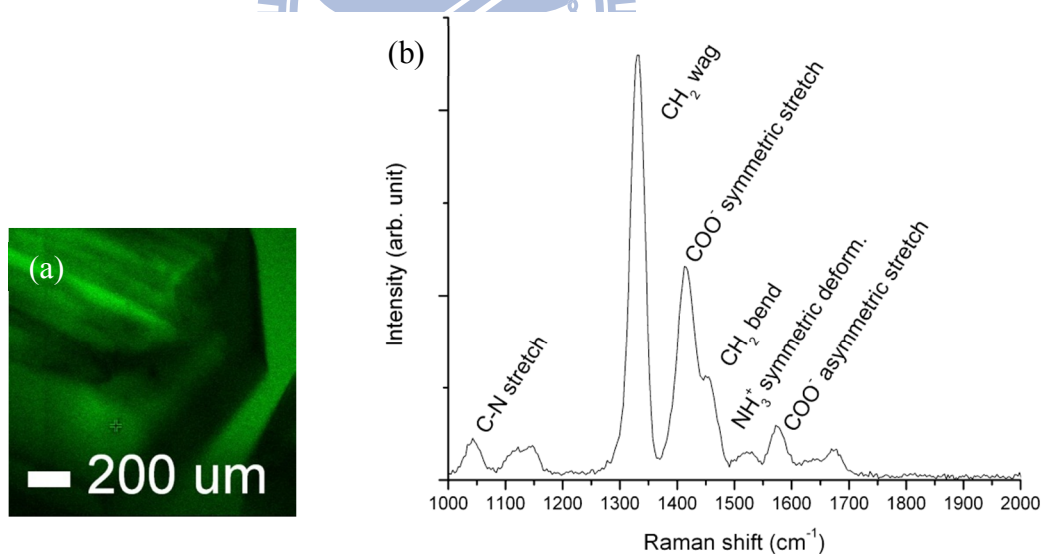
Fig. 4.10 (a) Raman image of obtained multiple crystals (b) Raman spectrum of obtained glycine crystal

4.2.6.2 Mass spectrometry

In order to confirm that neither photoreaction nor photo decomposition occurs during laser irradiation, the components of obtained crystals were analyzed by mass spectrometry (Quattro Micro, Micromass). The laser-induced crystals were redissolved with filtrated deionized water, and the obtained solution was compared with the glycine solution without laser irradiation. Since molecular weight of glycine is about 75, the peaks at mass-to-charge (m/z) ratio 76, 151.2 and 226.2 are ascribed to protonated glycine, protonated glycine adsorbed to another glycine molecule and protonated glycine adsorbed to another two glycine molecules, respectively. Mass spectrometry analysis suggests that the retention profile was in good agreement with that of glycine (Fig. 4.11). Namely, thermal product or photoproduct generated at the focal point, which could act like crystal nuclear as suggested by the
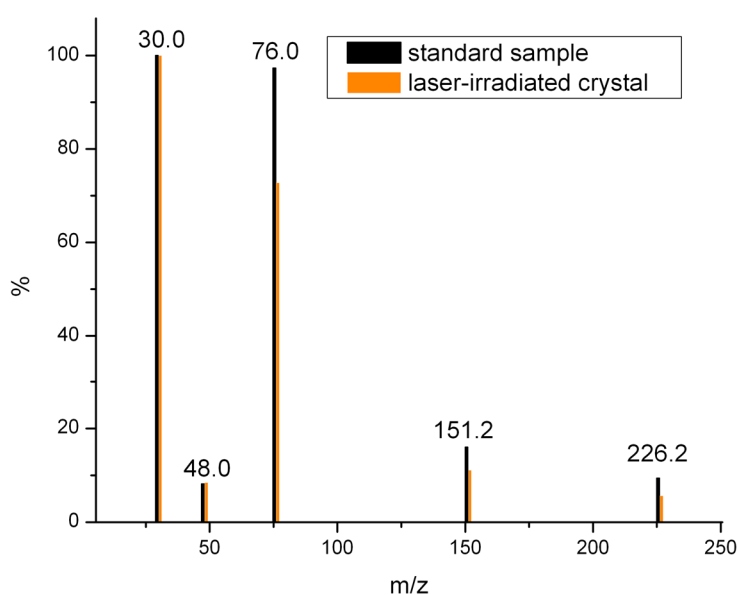
Fig. 4.11 Mass spectra of standard sample and laser-induced crystal.

photochemical crystallization [22, 24], was not detected in the crystals and appreciable thermal damage to crystal was also not found at this time even though the femtosecond laser can excite not only water but also glycine via multiphoton absorption [54]. The filtrated ionized water was also analyzed by mass spectrometry, and the intensity of the maximum signal is approximately two orders of magnitude weaker than that of glycine solution.

4.2.6.3 X-ray Analysis

X-ray analysis is the most authoritative method to determine lattice constants, crystallinity and crystalline phase. The obtained crystals of different morphologies same as the three samples measured in Raman spectroscopic measurement were analyzed again with X-ray diffraction measurement by Prof. Chun-Jung Chen and Mr. Ting-Wei Jiang in NSRRC, Hsinchu City, Taiwan. The wavelength of X-ray is about 1.54 Angstrom. In Table 4.1, it is shown that all of the obtained crystals are α-form and the result is consistent with Raman spectroscopic measurement. The crystal system is monoclinic and the space group is $P2_1/n$. Besides, there are 4 glycine molecules in one unit cell as shown in Fig. 4.12. It is also found that glycine molecule in crystal still keeps zwitterionic structure, $NH_3^+CH_2COO^-$. Two of the three hydrogen atoms attached to nitrogen atom form strong hydrogen bonds to oxygen atoms in the same layer and the third hydrogen atom shares its bond-forming capacity nearly equally between two nearest oxygen atoms in the adjacent layer [56].

Crystal morphology	a (Å)	b (Å)	c (Å)	α,γ (degree)	β (degree)	Cell volume (Å^3)	R-factor (%)
Single crystal	5.1055	11.9747	5.4638	90	111.742	310.276	3.15
Multiple crystal	5.1065	11.9774	5.4695	90	111.746	310.518	3.21
Powder-like crystal	5.1050	11.9763	5.4615	90	111.719	310.229	3.21
Reference [53]	5.102	11.970	5.457	90	111.42	309.6	

Table 4.1 The lattice constants and R-factors of glycine crystals with different morphologies.
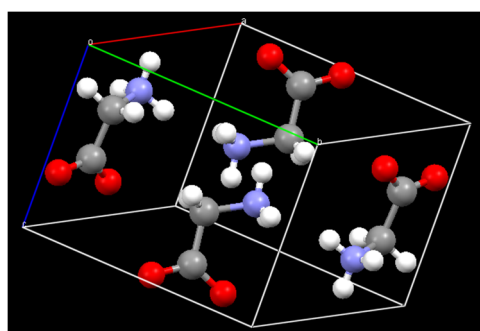
Fig. 4.12 Glycine molecules in one unit cell. (Single crystal case) It is ascribed to α-polymorph.

4.3 Discussion

4.3.1 Pulse energy dependence

The result reveals that the threshold of crystallization probability is closely related to that of cavitation bubble generation. In fact, Yoshikawa et al. has reported pulse energy dependence on femtosecond laser-induced nucleation of lysozyme recently. Based on their results, laser energies above the threshold of the cavitation bubble are required to induce protein nucleation [57]. It suggests that the cavitation bubble deformation such as expansion and shrinkage, and accompanying transient mechanical stress trigger nucleation of glycine as

demonstrated in previous works. Since crystallization did not take place when we irradiated the laser at low pulse energy below the threshold of cavitation bubble generation, the result also indicates that optical Kerr effect, which is one of essential explanations in nanosecond laser-induced crystallization, induced by femtosecond laser pulse is not dominant in this crystallization method [26, 58]. It is assumed that femtosecond pulse duration, 160 fs in this case, may be shorter than the time scale of molecular rotation and reorientation.

4.3.2 Repetition rate dependence

This result implies that the crystallization probability and crystal polymorph are strongly related to the number of irradiated pulses in a fixed period. The polymorph difference because of different repetition rates is explained by a schematic illustration shown in Fig. 4.13.
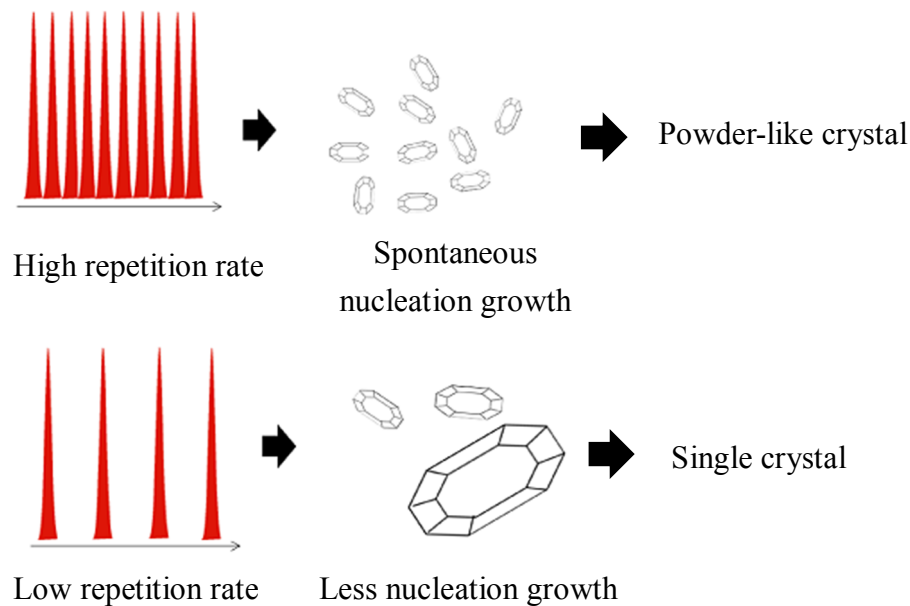
Fig. 4.13 Illustration to explain the morphology difference because of the different repetition rates.

At higher repetition rate, we consider that frequent nucleation caused by high repetition rate pulse trains can be regarded as homogeneous nucleation, resulting in simultaneous crystal growth and uniform crystal formation. Furthermore, to accelerate the narrow size distribution of powder-like crystals, we can raise a possibility that additional laser pulse irradiation to the formed crystals can cause crystal fragmentation via laser ablation. The ablation can decrease in crystal mean size and the fragments can act as nuclei. Here it should be noted again that we could find crystals during laser irradiation only in the case of powder-like crystal formation. To evaluate this explanation, we irradiated femtosecond pulses to already formed glycine crystal in solution in the bottle, and then we observed fragmentation of the crystal because of multiphoton absorption induced ablation considering from the absorption spectrum of glycine crystal [54]. This also supports that frequent pulse irradiation can increase total number of crystal and can reduce the mean size.

Conversely, low repetition rate pulse trains give lower probability of nucleation. It is relatively easier for nucleation to diffuse from the focal point because the interval of nucleation should be longer. This results in inhomogeneous distribution of crystal size, which can induce Ostwald ripening driven by surface energy reduction from smaller crystal to larger one, resulting in single crystal formation. This explanation is also consistent with the longer crystal formation period for single crystal mentioned above. Consequently, the results of this

repetition rate dependence can strongly suggest the possibility to obtain single crystal.

4.3.3 Focal position dependence

The present results can be possibly explained by two reasons. Firstly, we suppose that glycine molecules are adsorbed at the air/solution or solution/glass interface, and their alignment may be enhanced, decreasing free energy barrier to nucleation [59]. If molecular adsorption at the air/solution interface takes place, compared with the surface tension of pure solvent, it is expected that concentrated solution has relatively lower surface tension. Although only surface tension data of unsaturated glycine solution at the air/solution interface was reported and showed an slightly increasing tendency as concentration increased [60], it is believed that surface tension of supersaturated glycine solution may be much lower than that of pure water since clusters will be formed and be adsorbed at the air/solution interface.

Secondly, it is also explainable on the basis of the transient pressure around the cavitation bubble. When the femtosecond laser pulses are irradiated to the solution inside, the transient mechanical stress followed by cavitation bubble generation can be outspread to all the direction homogeneously. On the other hand, in the case of irradiation at the interfaces, the mechanical stress is localized and propagates inhomogeneously toward the interfaces, air/solution and solution/glass, and especially this phenomenon is more obvious at the

air/solution interface since the air/solution interface is a comparatively free interface. The localization of mechanical stress can enhance crystallization probability, and moreover this explanation should be coupled with the molecular adsorption at the air/solution interface.

4.4 Summary

In this work, femtosecond laser-induced crystallization of glycine has been studied in detail by changing various experimental parameters. Here we can propose that optimizing laser parameters and utilizing air/solution interface can give more sophisticated crystallization technique. Especially protein crystallization at the air/solution interface is highly expected because of the high crystallization probability, despite the fact that conformation change of protein may be simultaneously induced at the interfaces.
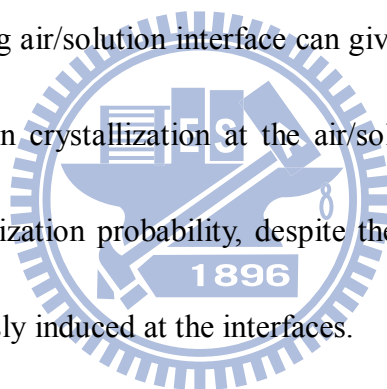
Chapter 5

Application to Protein

5.1 Introduction

Hen egg-white lysozyme (HEWL) is a fully sequenced enzyme that contains 129 amino acids inclusive of all 20 common amino acids, and has an elliptical molecular shape with approximate dimensions of $30 \times 30 \times 45$ Å^3 (Fig. 5.1) [61-63]. As one of globular proteins with a high degree of conformational stability and a low degree of flexibility, lysozyme is considered to be rigid and tend to resist large, irreversible changes in conformation [64]. Therefore, lysozyme is employed as a typical and easy-handling protein in biological studies.

From the point of view of molecular science, adsorption of proteins at interfaces has been a topic of increasing interest over the past several decades because of its importance in fields ranging from medical implantation and drug delivery to biological sensor fabrication. A variety of techniques have been employed to investigate adsorption behavior both at the solid/liquid and vapor/liquid interfaces. Lysozyme has received particular attention because its structural characteristics are well-understood at the molecular level and it has already allowed many of its adsorption properties to be elucidated [65]. Accordingly, adsorption behavior of

lysozyme leads to formation of locally higher concentration at the air/solution interface.

On the other hand, in the field of crystal chemistry, lysozyme has been widely studied in protein crystallization until now [19, 61]. Typical lysozyme crystal shows hexagonal shape as represented in Fig. 5.2 [14, 66]. Highly purified lysozyme powder is commercially available in large quantities at a modest cost [61]. In addition, lysozyme crystal can be grown easily and its crystallization condition is relatively simple. Lysozyme crystallization has been demonstrated by many light-induced crystallization methods inclusive of femtosecond laser-induced crystallization as mentioned before [10, 22, 34]. In fact, femtosecond-laser induced crystallization was first demonstrated with lysozyme [10]. To sum up, lysozyme is also chosen as a representative protein in this experiment to confirm the assumption that molecular adsorption at the air/solution interface much improves the crystallization probability with irradiation.
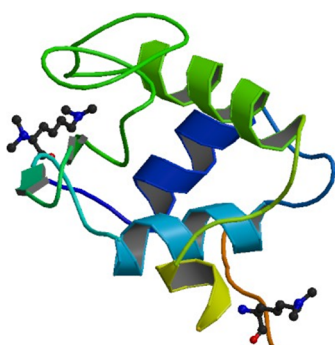
Fig. 5.1 Three-dimensional conformation of hen egg white lysozyme (HEWL) [61].
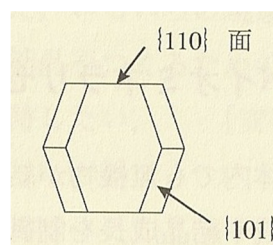
Fig. 5.2 The lysozyme crystal shape [14].

5.2 Results

5.2.1 Focal position dependence

In order to verify the significant improvement of crystallization when the laser is irradiated at the air/solution interface, spontaneous crystallization and irradiation inside the solution were also carried out simultaneously to be compared. Actually, the focal position of irradiation inside the solution was actually 0.5 mm below the air/solution interface since ablation of the crystallization plate takes place when the laser focal point is too close to the crystallization plate surface. That is also the reason why it is difficult to examine the crystallization probability with laser irradiation at the solution/solid interface. For each condition, more than 100 samples were examined and the results were shown in the form of crystallization probability. Pulse energy, irradiation time, and repetition rate were fixed to 10 μJ/pulse, 1 minute and 10 Hz, respectively. The concentration of NaCl as a crystallization agent was 10 mg/ml, which is about or even less than one third of normal concentration used in light-induced crystallization methods [10, 22, 34] and conventional crystallization methods [19].

Since the minimum crystallization time under laser irradiation is 3 days while it takes at least 7 days to crystallize spontaneously, in order to discuss the results fairly, a meaningful

time interval for observation is fixed in 7 days here. Figure 5.3 shows the crystallization

probabilities recorded at 7 days after laser irradiation. It is found that the crystallization

probability with irradiation at the air/solution interface is roughly two times higher than that

with irradiation inside the solution, and spontaneous crystallization gave the lowest

crystallization probability among these three conditions. Besides, it is observed that the

crystals obtained by laser irradiation at the air/solution interface or inside the solution are

larger, the size distribution is more homogeneous, and the shape is more complete and regular

on average compared with the crystals obtained by spontaneous crystallization. The crystal

number also shows difference. Usually, less than 10 crystals are more likely to be obtained by
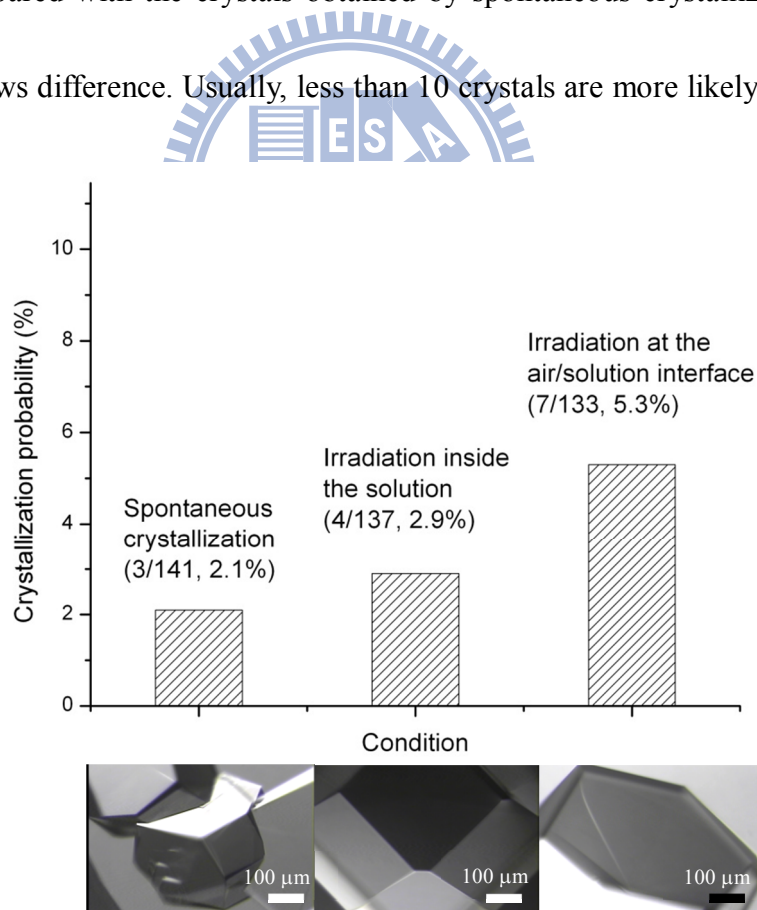
Fig. 5.3 Crystallization probabilities and crystal images of lysozyme under spontaneous crystallization, irradiation inside the solution and irradiation at the air/solution interface. (NaCl conc.: 10 mg/ml)

laser irradiation while the number of crystals crystallizing spontaneously is quite fluctuated.

In fact, all of the obtained crystals can be observed by naked eyes directly, and their size is

certainly large enough for further X-ray analysis. As demonstrated here, utilizing surface

irradiation efficiently improves the crystallization probability, and provides crystals with

shorter crystallization time, higher quality and larger size simultaneously.

5.2.2 Crystallization agent concentration dependence

Sodium chloride as a crystallization agent plays an important role in lysozyme

crystallization to reduce the solubility. However, an excess of sodium chloride can greatly

affect crystal quality. In this experiment, NaCl concentration was changed to 0, 2.5, 5, 7.5, 20

and 30 mg/ml, respectively. For each NaCl concentration, more than 40 samples were studied.
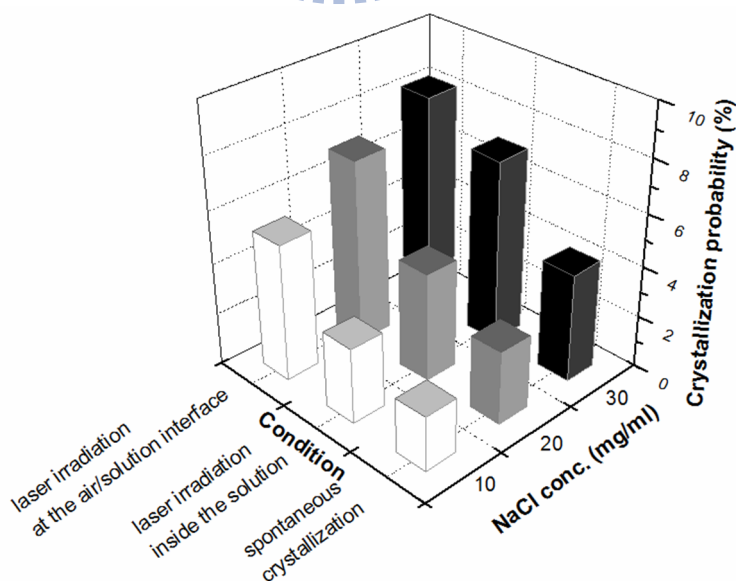
Fig. 5.4 Crystallization probabilities of lysozyme under spontaneous crystallization, irradiation inside the solution and irradiation at the air/solution interface. (NaCl conc.: 10, 20, 30 mg/ml)

Pulse energy, irradiation time, and repetition rate were fixed to 10 µJ/pulse, 1 minute and 10 Hz just as the previous experiment.

At former four lower NaCl concentrations (0, 2.5, 5, 7.5 mg/ml), lysozyme could not be crystallized even under laser irradiation at the air/solution interface during 7 days after laser irradiation. On the contrary, lysozyme crystals came at latter two higher NaCl concentrations, and the crystallization probabilities were improved under both of laser irradiation and spontaneous crystallization compared to that under the same conditions at original 10 mg/ml NaCl concentration. However, the probability difference between crystallization under laser irradiation at the air/solution interface and laser irradiation inside the solution becomes smaller.
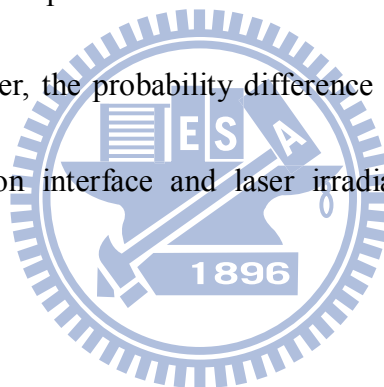
5.2.3 Characterization

X-ray analysis is utilized to determine the crystalline phase and the crystallinity of the obtained lysozyme crystals. Undoubtedly, information of molecular structure and sequence are also available. Based on the X-ray analysis result, differences among crystals crystallized spontaneously and laser-induced crystals under various experimental conditions will be discussed.

5.2.3.1 X-ray analysis

At first, an important difference between crystals of a small molecule and crystals of a protein should be mentioned. In protein crystals, the globular or egg-shaped molecules are loosely packed with large solvent-filled holes and channels, which normally occupy 40% to 60% of the crystal volume. Small reagent molecules can diffuse through these channels and reach reactive sites on all protein molecules in the crystal. However, the high solvent content causes problems in handling the crystals because loss of solvent destabilizes the crystals. Therefore, protein crystals should always be kept in their mother liquor, in the saturated vapor of their mother liquor, or at a sufficiently low temperature to prevent evaporation of the solvent [15].
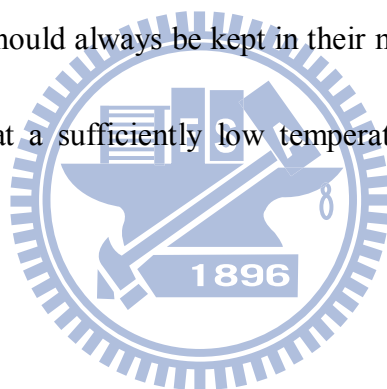
For protein such a large molecule, there are fewer molecules compared with crystal composed of small molecules in the same size. Besides, proteins consist mainly of light elements with only a few electrons per atom such as carbon, nitrogen and oxygen, so the light elements scatter X-rays much more weakly than heavy atoms. Since the diffracted intensity of protein crystal is much lower, a high intensity X-ray source is necessary to be used [15]. Therefore, X-ray source from synchrotron radiation is used in this study.

Lysozyme crystals obtained by spontaneous crystallization, laser irradiation at the

air/solution interface, and laser irradiation inside the solution at two different NaCl concentrations, 10 and 20 mg/ml, were analyzed by Prof. Chun-Jung Chen and Mr. Ting-Wei Jiang in NSRRC, Hsinchu City, Taiwan. Under each experimental condition except for spontaneous crystallization at 10 mg/ml, two crystals from different samples were picked with appropriate-sized loops from the solution. In order to prevent from loss or evaporation of water inside protein crystal, the obtained crystals were immersed into a mixture of mother liquor and glycerol in the volume ratio 4 to 1, and then were kept in liquid nitrogen before X-ray analysis. Glycerol is used as antifreeze to prevent water molecules inside the crystal frozen, and mother liquor is identical to 100 mM phosphate buffer solution in a concentrated NaCl solution. The resolution of X-ray was about 1.3 Angstrom.
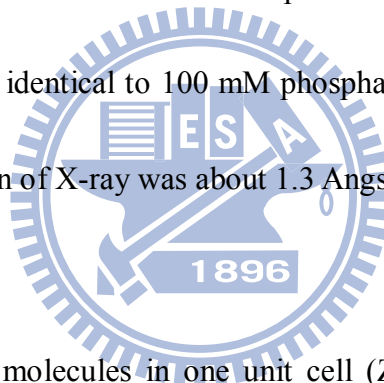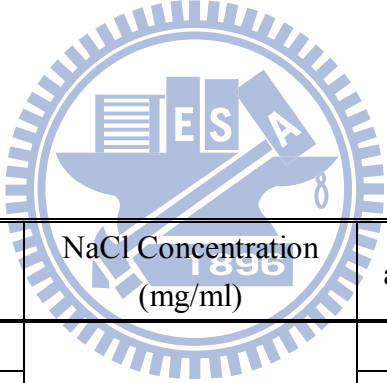
There are 8 lysozyme molecules in one unit cell (Z=8). It is found that the obtained lysozyme crystals under various experimental conditions show tetragonal (s.gr. $P4_32_12$) which is the same crystal system as shown in literature [14], quite similar lattice constants, and acceptable mosaicity (below 0.5) which is a numerical value indicating the degree of long-range order of the unit cells within a crystal. Since two crystals from different samples under the same experimental condition were examined, the results are also reproducible. The lattice constants are shown in Table 5.1, and three reconstructed lysozyme molecular structures under different laser conditions but at the same NaCl concentration, 10 mg/ml, are

illustrated by PyMOL software in Fig. 5.5.

Since there is no obvious difference among three molecular structures, electron density

distribution, a primitive data in real space derived from X-ray diffraction pattern and phase

information in reciprocal space by Fourier transform, is used for comparison in detail. In fact,

diffracted X-ray beams are strongly affected by electron density distribution. X-rays are

scattered almost exclusively by the electrons in the molecules but not by the nuclei. In other

words, the scattering is an interaction between X-rays as electromagnetic waves and the

electrons. If an electromagnetic wave is incident on a system of electrons, the electric and

magnetic components of the wave exert a force on the electron and make electrons oscillating

with the same frequency as the incident wave. These oscillating electrons acting as radiate

scatters first absorb energy and then emit radiation again [15]. From electron density

distribution, secondary structures such as α-helix and β-sheet can be easily identified and then

molecular structure at atomic scale can be reconstructed. If electron density distribution is

broken or discontinuous, it may indicate that the crystal lattices are slight different with each

other and may also cause some problems to give a correct protein molecular structure. After

refinement from electron density distribution to molecular structure is repeated several times,

more complete structure will be more likely to be obtained.

Electron density distribution shows some differences among spontaneous crystallization, laser irradiation at the air/solution interface, and laser irradiation inside the solution. For instance, in one of α-helices as a relatively flexible part of lysozyme shown in Fig. 5.6, it is found that spontaneous crystallization (blue) gives the most continuously distributed electron density while electron density of the crystal obtained by laser irradiation inside the solution (red) is most broken. However, in one of disulfide bonds as a relatively rigid part of lysozyme shown in Fig. 5.7, there is almost no difference among these three cases. Although the local electron density difference in one of α-helices is found, the structures are still almost the same and reproducible.

Experimental condition	NaCl Concentration (mg/ml)	a,b (Å)	c (Å)	α,β,γ (degree)
Spontaneous crystallization	10	78.552	37.008	90
Irradiation inside the solution		78.676	37.064	90
		78.250	37.033	90
Irradiation at the air/solution interface		78.800	37.081	90
		78.634	37.081	90
Spontaneous crystallization	20	78.553	36.957	90
		78.349	36.995	90
Irradiation at the air/solution interface		78.507	37.038	90
		78.793	37.087	90
Reference [14]		79.1	37.9	90

Table 5.1 The lattice constants of lysozyme crystals under various experimental conditions.
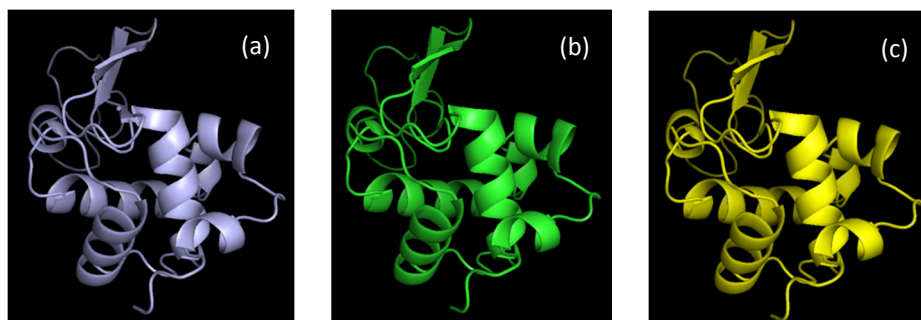
Fig. 5.5 The reconstructed lysozyme molecular structures from the X-ray analysis data under different laser conditions but at the same NaCl concentration, 10 mg/ml. (a) Spontaneous crystallization (b) Irradiation inside the solution (c) Irradiation at the air/solution interface
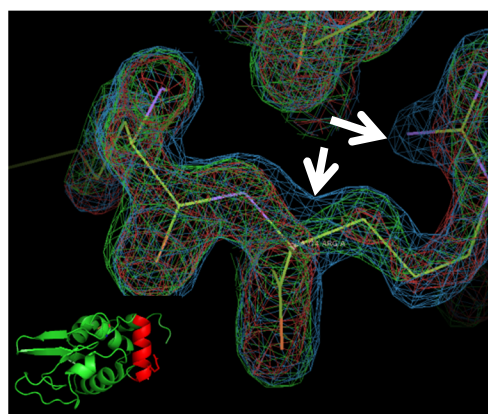
Fig. 5.6 Electron density distribution of one of α-helices under different laser conditions but at the same NaCl concentration, 10 mg/ml. (blue) Spontaneous crystallization (red) Irradiation inside the solution (green) Irradiation at the air/solution interface
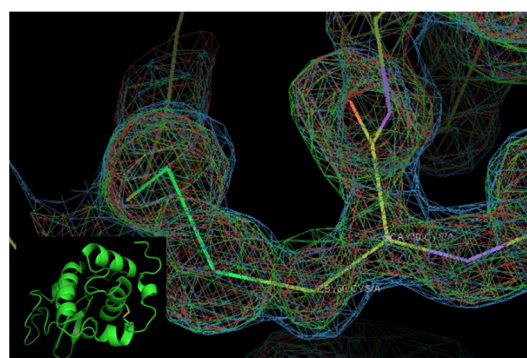
Fig. 5.7 Electron density distribution of one of disulfide bonds under different laser conditions but at the same NaCl concentration, 10 mg/ml. (blue) Spontaneous crystallization (red) Irradiation inside the solution (green) Irradiation at the air/solution interface

5.3 Surface tension measurement

In order to confirm that molecular adsorption at the air/solution interface occurs and improves crystallization probability, surface tension of lysozyme solutions at different lysozyme concentrations and salt concentrations were measured. The facility for surface
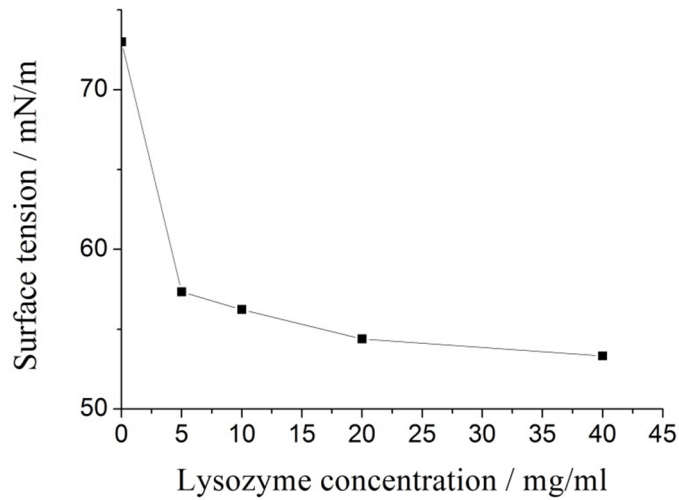
Fig. 5.8 Lysozyme concentration (mg/ml) dependence on surface tension (mN/m^2). Lysozyme concentrations are 0, 5 10, 20 and 40 mg/ml, respectively. NaCl concentration is fixed to 20 mg/ml.
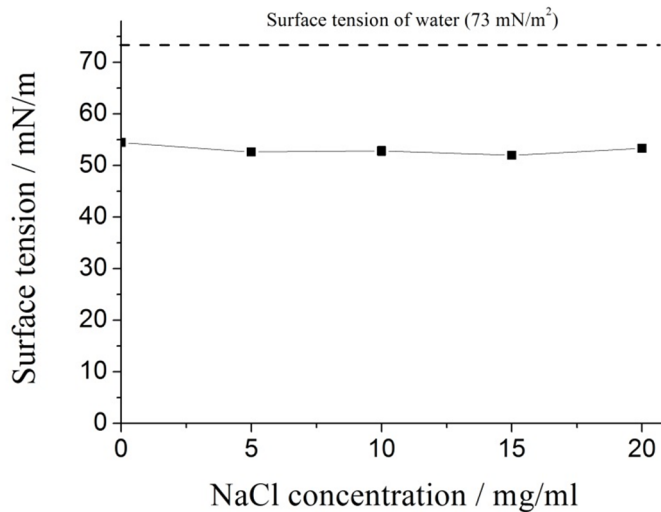
Fig. 5.9 NaCl concentration (mg/ml) dependence on surface tension (mN/m^2). NaCl concentrations are 0, 5, 10, 15 and 20 mg/ml, respectively. Lysozyme concentration is fixed to 40 mg/ml.

tension measurement was established by Prof. Yohko F. Yano in Kinki University, Osaka,

Japan, and the programming and the measurements were carried out by Dr. Takayuki Uwada

in our laboratory. As a result, with increasing lysozyme concentration from 0 to 40 mg/ml, the

surface tension decreased apparently (Fig. 5.8). However, the surface tension did not change

much with increasing salt concentration from 5 to 20 mg/ml (Fig. 5.9). The constant surface

tension drop is attributed to fixed high lysozyme concentration.

5.4 Discussion

It is observed that irradiation at the air/solution interface of the lysozyme solution droplet

improved the crystallization probability very much, compared with that of spontaneous

crystallization. The finding may be attributed to surface adsorption of lysozyme. The surface

active behavior of proteins was found and is frequently employed in medicine and industry.

The adsorption of proteins at an interface is accompanied by changes in the physical

properties of the interface, particularly its interfacial tension. Moreover, it induces
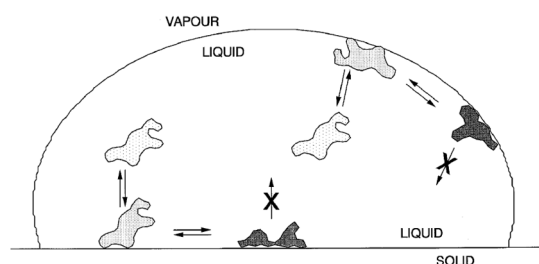
Fig. 5.10 Conformation changes of protein
take place at interfaces [67].

conformational changes of proteins at the interface (Fig. 5.10) [67]. Lysozyme molecules

initially adsorbed on the air/solution interface have a flat unfolding structure, forming

antiparallel β-sheets as a result of hydrophobic interactions with the gas phase [63]. Therefore,

sodium chloride as a crystallization agent is added to decrease lysozyme solubility and to

keep refolding structure stabilized at the air/solution interface by salting out (Fig. 5.11) [68].

The results of surface tension measurement also support that coverage of lysozyme

molecules at the air/solution interface increases with lysozyme concentration and the amount

of salt does not interfere with molecular adsorption behavior of lysozyme at the interface. It

can be regarded as a direct evidence of molecular adsorption at the air/solution interface.

Although it has been reported that molecular adsorption at the air/solution interface takes

several hours to reach steady-state equilibrium at three relatively lower concentrations, 0.01,

0.1 and 1.0 mg/ml, the necessary time may be greatly reduced in our case since the used

lysozyme concentration is much higher than that demonstrated in literature [64].
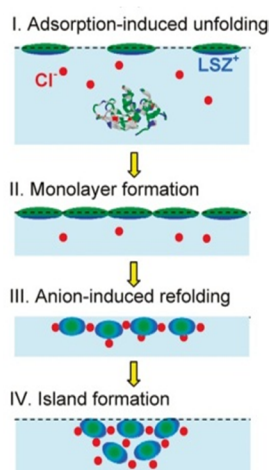
Fig. 5.11 Salting out can keep lysozyme molecules refolding and can localize them even at the air/solution interface [68].

In X-ray diffraction analysis, there is almost no difference in the crystalline phase and the mosaicity between crystals given by spontaneous crystallization and laser irradiation. Although further analysis revealed that the local electron density in one of α-helices is slightly different, the overall molecular structures are still almost the same and reproducible.

5.5 Summary

The crystallization probability improvement of lysozyme crystallization by focusing a femtosecond laser beam at the air/solution interface is demonstrated. It is attributed to lysozyme adsorption at the air/solution interface and has been confirmed by surface tension measurement. Although surface adsorption of protein induces the morphological change, previous reports suggested that lysozyme structure is stabilized at the air/solution interface by salting-out effect. X-ray diffraction also revealed that all the crystals under each condition show identical crystal structure.

Chapter 6

Conclusion

In this study, we explored how femtosecond laser parameters such as pulse energy, repetition rate and focal position affect crystallization and obtained crystals, and then demonstrated that solution surface irradiation of femtosecond laser pulses can improve molecular crystallization probability drastically. Firstly, femtosecond laser induced crystallization of glycine from supersaturated aqueous solution is demonstrated and relations between laser parameters and crystallization probability, crystal morphology and polymorph are examined. Pulse energy and repetition rate dependences show that the frequency of cavitation bubble generation induced by multiphoton absorption of water mainly determines crystal morphology and number. Furthermore, significant increase of crystallization probability is also demonstrated by focusing femtosecond pulses at the air/solution interface, whose mechanism may be ascribed to molecular adsorption at the interface. Consequently, we have succeeded in single glycine crystal formation induced by single femtosecond pulse irradiation for the first time as far as we know.

Secondly, we demonstrate femtosecond laser induced crystallization of lysozyme as the

most standard protein in protein crystallography in the similar manner to glycine. It is revealed that irradiation at the air/solution interface of the solution droplet much improved the crystallization probability, compared with that of femtosecond laser irradiation inside the solution and that of spontaneous crystallization. X-ray diffraction analysis of the obtained crystals clarified that crystal structures were identical in each crystallization condition. It is known that protein can be adsorbed and be localized at the solution surface in spite of the denaturation. However, this result indicates that the salting-out effect can stabilize the structure even at the surface, which is contemporarily reported in elsewhere.

To sum up, the present result clearly suggests that utilizing solution surface irradiation in femtosecond laser-induced crystallization sharpens the existent protein crystallization technique.
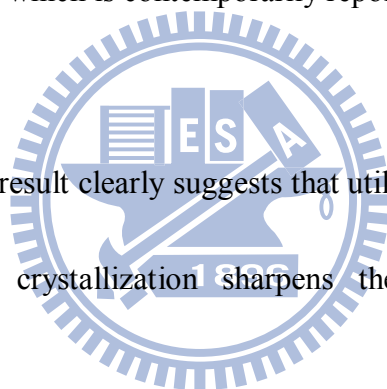
Chapter 7

Spectroscopic Investigation on Tsunami Crystallization and Role of Interface, and Future Scope

Further spectroscopic dynamics study on the early stage of molecular nucleation occurring at the surface is promising to establish novel interface/surface molecular science from this crystallization methodology. Since a protocol for lysozyme crystallization is known and the improvement of crystallization probability has been demonstrated in this study, crystallization of modified lysozyme such as lysozyme with a sugar may be worth trying. On the other hand, femtosecond laser-induced crystallization method combined with trapping laser will also be a practical methodology to improve crystallization probability more. Undoubtedly, from the view point of biology and pharmaceutics, the most attractive application is to crystallize more proteins and solve their unknown molecular structure.

Reference

1. 日本分光学会, 分光測定のためのレーザー入門, 1st ed., 講談社, 2009.

2. Y. Kawamura, K. Toyota, and S. Namba, "Effective deep ultraviolet photoetching of polymethyl methacrylate by an excimer laser", Appl. Phys. Lett., **40** (5), 374 (1982)

3. R. Srinivasan and V. Mayne-Banton, "Self-developing photoetching of poly(ethylene terephthalate) films by farultraviolet excimer laser radiation", Appl. Phys. Lett., **41** (6), 576 (1982)

4. R. Srinivasan and W. J. Leigh, "Ablative Photodecomposition: Action of Far-Ultraviolet (193 nm) Laser Radiation on Poly(ethylene terephthalate) Films", J. Am. Chem. Soc., **104**, 6784 (1982)

5. Y. Jiang, Y. Matsumoto, Y. Hosokawa, H. Masuhara, and I. Oh, "Trapping and manipulation of a single micro-object in solution with femtosecond laser-induced mechanical force", Appl. Phys. Lett., **90**, 061107 (2007)

6. K. Konig, I. Riemann, and W. Fritzsche, "Nanodissection of human chromosomes with near-infrared femtosecond laser pulses", Opt. Lett., **26** (11), 819 (2001)

7. U. K. Tirlapur and K. Konig, "Cell biology: Targeted transfection by femtosecond laser", Nature, **418** (6895), 290 (2002)

8. T. Kaji, S. Ito, H. Miyasaka, Y. Hosokawa, H. Masuhara, C. Shukunami, and Y. Hiraki, "Nondestructive micropatterning of living animal cells using focused femtosecond laser-induced impulsive force", Appl. Phys. Lett., **91** (2), 023904 (2007)

9. A. Yamaguchi, Y. Hosokawa, G. Louit, T. Asahi, C. Shukunami, Y. Hiraki, and H. Masuhara, "Nanoparticle injection to single animal cells using femtosecond laser-induced impulsive force", Appl. Phys. A: Mater., **93** (1), 39 (2008)

10. H. Adachi, K. Takano, Y. Hosokawa, T. Inoue, Y. Mori, H. Matsumura, M. Yoshimura, Y. Tsunaka, M. Morikawa, S. Kanaya, H. Masuhara, Y. Kai, and T. Sasaki, "Laser Irradiated Growth of Protein Crystal", Jpn. J. Appl. Phys., **42** (Part 2, No. 7B), L798 (2003)

11. Y. Hosokawa, H. Adachi, M. Yoshimura, Y. Mori, T. Sasaki, and H. Masuhara, "Femtosecond Laser-Induced Crystallization of 4-(Dimethylamino)-N-methyl-4-stilbazolium Tosylate", Cryst. Growth Des., **5** (3), 861 (2005)

12. H. Y. Yoshikawa, Y. Hosokawa, and H. Masuhara, "Explosive Crystallization of Urea Triggered by Focused Femtosecond Laser Irradiation", Jpn. J. Appl. Phys., **45** (1), L23 (2006)

13. K. Nakamura, Y. Hosokawa, and H. Masuhara, "Anthracene Crystallization Induced by Single-Shot Femtosecond Laser Irradiation: Experimental Evidence for the Important Role of Bubbles″, Cryst. Growth Des., **7** (5), 885 (2007)

14. 平山令明, 有機化合物結晶作製ハンドブック, 3rd ed., 丸善, 2010.

15. J. Drenth, *Principles of protein x-ray crystallography*. 2007, Springer: New York.

16. A. N. Azadani, J. M. Lopez, and A. H. Hirsa, "Protein Crystallization at the Air/Water Interface Induced by Shearing Bulk Flow″, Langmuir, **23** (10), 5227 (2007)

17. R. Murai, H. Y. Yoshikawa, H. Kawahara, S. Maki, S. Sugiyama, T. Kitatani, H. Adachi, K. Takano, H. Matsumura, S. Murakami, T. Inoue, T. Sasaki, and Y. Mori, "Effect of solution flow produced by rotary shaker on protein crystallization″, J. Cryst. Growth, **310** (7-9), 5 (2008)

18. M. Caffrey, "Membrane Protein Crystallization″, J. Struct. Biol., **142** (1), 25 (2003)

19. A. McPherson, Crystallization of Biological Macromolecules, 1st ed., CSHL PRESS, 1999.

20. P. G. Vekilov, "Dense Liquid Precursor for the Nucleation of Ordered Solid Phases from Solution″, Cryst. Growth Des., **4** (4), 671 (2004)

21. T. Okutsu, K. Isomura, N. Kakinuma, H. Horiuchi, M. Unno, H. Matsumoto, and H. Hiratsuka, "Laser-Induced Morphology Control and Epitaxy of Dipara-anthracene Produced from the Photochemical Reaction of Anthracene″, Cryst. Growth Des., **5** (2), 461 (2004)

22. T. Okutsu, K. Furuta, M. Terao, H. Hiratsuka, A. Yamano, N. Ferte, and S. Veesler, "Light-Induced Nucleation of Metastable Hen Egg-White Lysozyme Solutions″, Cryst. Growth Des., **5** (4), 1393 (2005)

23. T. Okutsu, K. Sugiyama, K. Furuta, I. Watanebe, H. Mori, K. Obi, K. Horota, H. Horiuchi, G. Sazaki, S. Veesler, and H. Hiratsuka, "Photochemically induced nucleation in supersaturated and undersaturated thaumatin solutions″, J. Photoch. Photobio. A, **190** (1), 88 (2007)

24. K. Furuta, H. Horiuchi, H. Hiratsuka, and T. Okutsu, "Photochemically Induced Nucleation of Ribonuclease A Enhanced by a Stable Protein Dimer Produced from the Photochemical Reaction of Tyr Residual Groups″, Cryst. Growth Des., **8** (6), 1886 (2008)

25. B. A. Garetz, J. E. Aber, N. L. Goddard, R. G. Young, and A. S. Myerson, "Nonphotochemical, Polarization-Dependent, Laser-Induced Nucleation in Supersaturated Aqueous Urea Solutions″, Phys. Rev. Lett., **77** (16), 3475 (1996)

26. B. A. Garetz, J. Matic, and A. S. Myerson, "Polarization Switching of Crystal Structure in the Nonphotochemical Light-Induced Nucleation of Supersaturated Aqueous Glycine Solutions″, Phys. Rev. Lett., **89** (17), 175501 (2002)

27. X. Sun, B. A. Garetz, and A. S. Myerson, "Supersaturation and Polarization Dependence of Polymorph Control in the Nonphotochemical Laser-Induced

Nucleation (NPLIN) of Aqueous Glycine Solutions″, <u>Cryst. Growth Des.</u>, **6** (3), 684 (2006)

28. J. E. Aber, S. Arnold, B. A. Garetz, and A. S. Myerson, "Strong dc Electric Field Applied to Supersaturated Aqueous Glycine Solution Induces Nucleation of the gamma Polymorph″, <u>Phys. Rev. Lett.</u>, **94** (14), 145503 (2005)

29. A. Ashkin, J. M. Dziedzic, J. E. Bjorkholm, and S. Chu, "Observation of a single-beam gradient force optical trap for dielectric particles″, <u>Opt. Lett.</u>, **11** (5), 288 (1986)

30. V.-D. Tuan, *Biomedical Photonics Handbook*. Optical Properties of Tissue, M. Joel and V.-D. Tuan. 2003, CRC Press: Boca Raton.

31. T. Sugiyama, T. Adachi, and H. Masuhara, "Crystallization of Glycine by Photon Pressure of a Focused CW Laser Beam″, <u>Chem. Lett.</u>, **36** (12), 1480 (2007)

32. T. Rungsimanon, K. Yuyama, T. Sugiyama, H. Masuhara, N. Tohnai, and M. Miyata, "Control of Crystal Polymorph of Glycine by Photon Pressure of a Focused Continuous Wave Near-Infrared Laser Beam″, <u>J. Phys. Chem. Lett.</u>, **1** (3), 599 (2010)

33. K. Yuyama, T. Sugiyama, and H. Masuhara, "Millimeter-Scale Dense Liquid Droplet Formation and Crystallization in Glycine Solution Induced by Photon Pressure″, <u>J. Phys. Chem. Lett.</u>, **1** (9), 1321 (2010)

34. Y. Tsuboi, T. Shoji, and N. Kitamura, "Crystallization of Lysozyme Based on Molecular Assembling by Photon Pressure″, <u>Jpn. J. Appl. Phys.</u>, **46** (49), L1234 (2007)

35. Y. Tsuboi, T. Shoji, and N. Kitamura, "Optical Trapping of Amino Acids in Aqueous Solutions″, <u>J. Phys. Chem. C</u>, **114** (12), 5589 (2010)

36. N. Iefuji, R. Murai, M. Maruyama, Y. Takahashi, S. Sugiyama, H. Adachi, H. Matsumura, S. Murakami, T. Inoue, Y. Mori, Y. Koga, K. Takano, and S. Kanaya, "Laser-induced nucleation in protein crystallization: Local increase in protein concentration induced by femtosecond laser irradiation″, <u>J. Cryst. Growth</u>, **318** (1), 741 (2011)

37. J.-L. Boulnois, "Photophysical processes in recent medical laser developments: A review ″, <u>Laser Med. Sci.</u>, **1**, 47 (1986)

38. A. Vogel and V. Venugopalan, "Mechanisms of Pulsed Laser Ablation of Biological Tissues″, <u>Chem. Rev.</u>, **103** (2), 577 (2003)

39. A. Vogel, S. Busch, and U. Parlitz, "Shock wave emission and cavitation bubble generation by picosecond and nanosecond optical breakdown in water ″, <u>J. Acoust. Soc. Am.</u>, **100** (1), 148 (1996)

40. L. Rayleigh, "On the pressure developed in a liquid during the collapse of a spherical cavity″, <u>Philos. Mag.</u>, **34** (200), 94 (1917)

41. T. Juhasz, G. A. Kastis, C. Suarez, Z. Bor, and W.E. Bron, "Time-Resolved Observations of Shock Waves and Cavitation Bubbles Generated by Femtosecond

Laser Pulses in Corneal Tissue and Water″, <u>Laser. Surg. Med.</u>, **19** (1), 23 (1996)

42. R. Murai, H. Y. Yoshikawa, Y. Takahashi, M. Maruyama, S. Sugiyama, G. Sazaki, H. Adachi, K. Takano, H. Matsumura, S. Murakami, T. Inoue, and Y. Mori, "Enhancement of femtosecond laser-induced nucleation of protein in a gel solution″, <u>Appl. Phys. Lett.</u>, **96** (4), 043702 (2010)

43. K. Nakamura, Y. Sora, H. Y. Yoshikawa, Y. Hosokawa, R. Murai, H. Adachi, Y. Mori, T. Sasaki, and H. Masuhara, "Femtosecond laser-induced crystallization of protein in gel medium″, <u>Appl. Surf. Sci.</u>, **253**, 6425 (2007)

44. A. Soare, R. Dijkink, M. R. Pascual, C. Sun, P. W. Cains, D. Lohse, A. I. Stankiewicz, and H. J. M. Kramer, "Crystal Nucleation by Laser-Induced Cavitation″, <u>Cryst. Growth Des.</u>,   (2011)

45. Data sheet from CBC Optics Co., Ltd.

46. P. L. d. Noüy, "AN INTERFACIAL TENSIOMETER FOR UNIVERSAL USE″, <u>J. Gen. Physiol.</u>, **7** (5), 625 (1925)

47. J. Drelich, C. Fang, and C. L. White, *MEASUREMENT OF INTERFACIAL TENSION IN FLUID-FLUID SYSTEMS*. 2nd ed. 2002, Taylor & Francis: New York.

48. W. D. Harkins and H. F. Jordan, "A Method for the Determination of Surface And Interfacial Tension from the Maximum Pull on a Ring″, <u>J. Am. Chem. Soc.</u>, **52**, 1751 (1930)

49. J. W. Mullin, <u>Crystallization</u>, 3rd ed., Butterworth-Heinemann Ltd., Oxford, 1993.

50. 中村和彦, "タンパク質および有機分子のフェムト秒レーザー誘起結晶化過程に関する研究″, <u>大阪大学</u>, 博士論文, (2007)

51. E. Cacioppo and M. L. Pusey, "The solubility of the tetragonal form of hen egg white lysozyme from pH 4.0 to 5.4″, <u>J. Cryst. Growth</u>, **114** (3), 286 (1991)

52. E. V. Boldyreve, V. A. Drebushchak, T. N. Drebushchak, I. E. Paukov, Y. A. Kovalevskaya, and E. S. Shutova, "POLOMORPHISM OF GLYCINE Thermodynamics aspects. Part I. Relative stability of the polymorphs″, <u>J. Therm. Anal. Calorim.</u>, **73**, 409 (2003)

53. Y. Iitaka, "The Crystal Structure of gamma-Glycine″, <u>Acta Crystallogr.</u>, **14**, 1 (1961)

54. K. Srinivasan, "Crystal growth of [alpha] and [gamma] glycine polymorphs and their polymorphic phase transformations″, <u>J. Cryst. Growth</u>, **311** (1), 156 (2008)

55. X. Yang, J. Lu, X. Wang, and C. B. Ching, "In situ monitoring of the solution-mediated polymorphic transformation of glycine: characterization of the polymorphs and observation of the transformation rate using Raman spectroscopy and microscopy″, <u>J. Raman Spectrosc.</u>, **39** (10), 1433 (2008)

56. G. Albrecht and R. B. Corey, "The Crystal Structure of Glycine″, <u>J. Am. Chem. Soc.</u>, **61** (5), 1087 (1939)

57. H. Y. Yoshikawa, R. Murai, S. Maki, T. Kitatani, S. Sugiyama, G. Sazaki, H. adachi, T. Inoue, H. matsumura, K. Takano, S. murakami, T. Sasaki, and Y. Mori, "Laser energy

dependence on femtosecond laser-induced nucleation of protein″, Appl. Phys. A: Mater., **93**, 911 (2008)

58. J. Zaccaro, J. Matic, A. S. Myerson, and B. A. Garetz, "Nonphotochemical, Laser-Induced Nucleation of Supersaturated Aqueous Glycine Produces Unexpected [gamma]-Polymorph″, Cryst. Growth Des., **1** (1), 5 (2001)

59. A. Sugimura, M. Iwamoto, and O.-Y. Zhong-can, "Phase transition of molecular orientation at the liquid-air interface″, Phys. Rev. E, **50** (1), 614 (1994)

60. L. M. Pegram and M. T. J. Record, "Using Surface Tension Data to Predict Differences in Surface and Bulk Concentrations of Nonelectrolytes in Water″, J. Phys. Chem. C, **113** (6), 2171 (2009)

61. W. R. Rypniewski, H. M. Holden, and I. Rayment, "Structural Consequences of Reductive Methylation of Lysine Residues in Hen Egg White Lysozyme: An X-ray Analysis at 1.8-Angstrom Resolution″, Biochemistry, **32**, 9851 (1992)

62. J. R. Lu, T. J. Su, and B. J. Howlin, "The Effect of Solution pH on the Structural Conformation of Lysozyme Layers Adsorbed on the Surface of Water″, J. Phys. Chem. B, **103** (28), 5903 (1999)

63. Y. F. Yano, T. Uruga, H. Tanida, H. Toyokawa, Y. Terada, M. Takagaki, and H. Yamada, "Driving Force Behind Adsorption-Induced Protein Unfolding: A Time-Resolved X-ray Reflectivity Study on Lysozyme Adsorbed at an Air/Water Interface″, Langmuir, **25** (1), 32 (2009)

64. B. C. Tripp, J. J. Magda, and J. D. Andrade, "Adsorption of Globular Proteins at the Air/Water Interface as Measured via Dynamic Surface Tension: Concentration Dependence, Mass-Transfer Considerations, and Adsorption Kinetics″, J. Colloid Interf. Sci., **173**, 16 (1994)

65. G. Kim, M. Gurau, J. Kim, and P. S. Cremer, "Investigations of Lysozyme Adsorption at the Air/Water and Quartz/Water Interfaces by Vibrational Sum Frequency Spectroscopy″, Langmuir, **18** (7), 2807 (2002)

66. Y. Tanimoto, R. Yamaguchi, Y. Kanazawa, and M. Fujiwara, "Magnetic orientation of lysozyme crystals″, RIKEN Review, **44**, 162 (2002)

67. W. v. d. Vegt, W. Norde, H. C. v. d. Mei, and H. J. Busscher, "Kinetics of Interfacial Tension Changes during Protein Adsorption from Sessile Droplets on FEP–Teflon″, J. Colloid Interf. Sci., **179** (1), 57 (1996)

68. Y. F. Yano, T. Uruga, H. Tanida, Y. Tereda, and H. Yamada, "Protein Salting Out Observed at an Air-Water Interface″, J. Phys. Chem. Lett., **2**, 995 (2011)